A 35-GHz Beam Waveguide System for the Millimeter-Wave Radar

William D. Fitzgerald

The millimeter-wave radar is a broadband, dual-polarized Cassegrain system operating in the Ka band (35 GHz) and W band (95 GHz). To upgrade system sensitivity and bandwidth, we replaced the 35-GHz microwave system with a reflecting beam waveguide (BWG), which is a quasi-optical system. This article describes the design and performance of the BWG retrofit. The goal is to increase sensitivity of the millimeter-wave radar by 10 dB. Two new high-power amplifiers, each of which produces double the power of the existing source, are paralleled with a quasi-optical combiner for a 6-dB increase in total power (to 100 kW). In addition, the BWG system reduces the microwave transmit-and-receive line losses by 4 dB. The new BWG system is the first quasi-optical, high-power, dual-polarized, angle-tracking radar; its advantages include lower losses, broader bandwidths, and power levels well beyond the capabilities of conventional waveguide systems. In particular, the quasi-optical components are superior to their waveguide counterparts. As a rule of thumb, if the main aperture in a Cassegrain system is greater than 400 wavelengths, then a BWG system becomes a viable option.

THE MILLIMETER-WAVE RADAR (MMW) is one of a group of radars at the Kiernan Reentry Measurements Systems (KREMS) facility located on Kwajalein Atoll in the Marshall Islands. KREMS is managed by Lincoln Laboratory under the sponsorship of the United States Army Kwajalein Atoll [1]. The MMW is a two-frequency system, or two quasi-independent radars, operating at Ka band (35 GHz) and W band (95 GHz). The antenna is a parabolic dish that uses Cassegrain optics with a vertex feed cluster made up of a 35-GHz multimode monopulse horn and a 95-GHz single-beam feed. Associated microwave components and receiver front ends are also included in the feed cluster. Figure 1 shows the radome that encloses and protects the MMW radar antenna, pedestal, and support tower from the corrosive Kwajalein environment. Table 1 lists the characteristic parameters of the MMW radar.

The principal functions of the MMW radar include high-resolution reentry-vehicle and wake measurements, satellite and reentry-vehicle imaging, and precise determination of metric data. A continuing effort is currently in progress to enhance the sensitivity of the MMW radar in support of these functions. A substantial increase in the single-pulse sensitivity of the system can be achieved only by some combination of reduced microwave losses and increased power radiated. This need for enhanced sensitivity spurred the development of the beam waveguide (BWG) system.

Highly directive Cassegrain antenna systems can utilize the advantages of feed systems based on quasi-optical propagation, or free-space propagation with a beam of manageable size. We are primarily concerned with the fundamental (pure Gaussian) mode of propagation, although higher-order Hermite-Gaussian

Table 1. Characteristics of the Millimeter-Wave Radar

Antenna diameter	13.7 m	
Frequency	35 GHz	95.5 GHz
Beamwidth	760 μrad	280 μrad
Peak power	25 kW	6 kW
Bandwidth	1000 MHz	1000 MHz
S/N on 1-square-mile target at 1000-km range	22 dB	3 dB

modes are used for monopulse angle tracking. All Gaussian modes, unlike their waveguide counterparts, have a free-space wavelength throughout, from the beam waist to the far field. Consequently, BWG systems are free of distortions. By using lenses or mirrors, we can refocus the diverging beam periodically. Corresponding transverse planes after each refocusing, or *iteration*, have identical amplitude and phase distributions. A BWG is, by definition, a configuration of lenses and/or mirrors that, by using this iteration process, results in low-loss propagation over a distance. C. Goubau et al. described a BWG using lenses [2], and J.E. Degenford built a reflective BWG using elliptic paraboloidal reflectors [3]. A number of large antenna systems for satellite ground stations have successfully utilized reflector BWG feeds that typically use a four-mirror configuration to transfer power from a transmitter at ground level to a virtual image at the focal point of a Cassegrain antenna [4, 5]. In addition to reducing propagation losses, the four-mirror configuration has the symmetry to function as azimuth and elevation rotary joints.

FIGURE 1. The millimeter-wave (MMW) radar at the Kiernan Reentry Measurements Systems facility on Kwajalein Atoll in the Marshall Islands. The radome protects the radar antenna from the corrosive island environment.

Not all radars are suitable for BWG systems. The aperture size in wavelengths, or D/λ, of the antenna system is the basic parameter that determines when the physical size of the BWG package makes it a viable alternative to a conventional microwave approach. MMW radar systems, which typically have electrically large apertures, are generally compatible with BWG systems.

A BWG system for a radar requires a number of quasi-optical components to replace their microwave equivalents. The 35-GHz system is a high-power angle-tracking radar with polarization flexibility (i.e., it transmits one circular sense and receives both), which requires components such as quasi-optical cir-

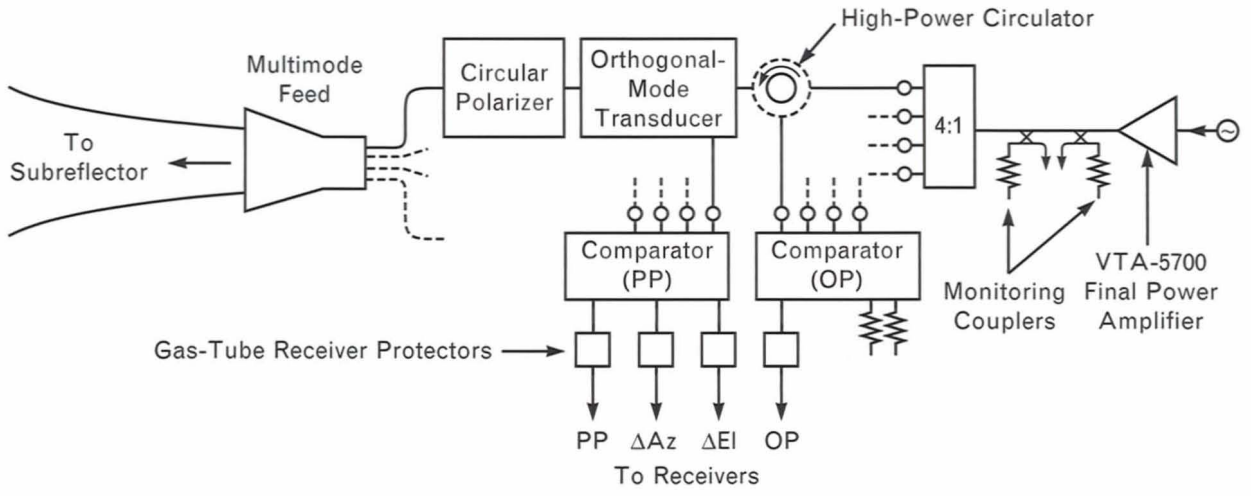

FIGURE 2. The 35-GHz microwave system that was replaced by a beam waveguide (BWG) system.

culator duplexers, circulator polarizers, and polarization filters. Figure 2 illustrates the component layout in the 35-GHz microwave system. A circularly polarized signal is radiated, and two circular senses—the preferred polarization (PP) and the opposite polarization (OP)—are received. Angle tracking is accomplished with the PP return.

Figure 3 shows a diagram of a BWG system with

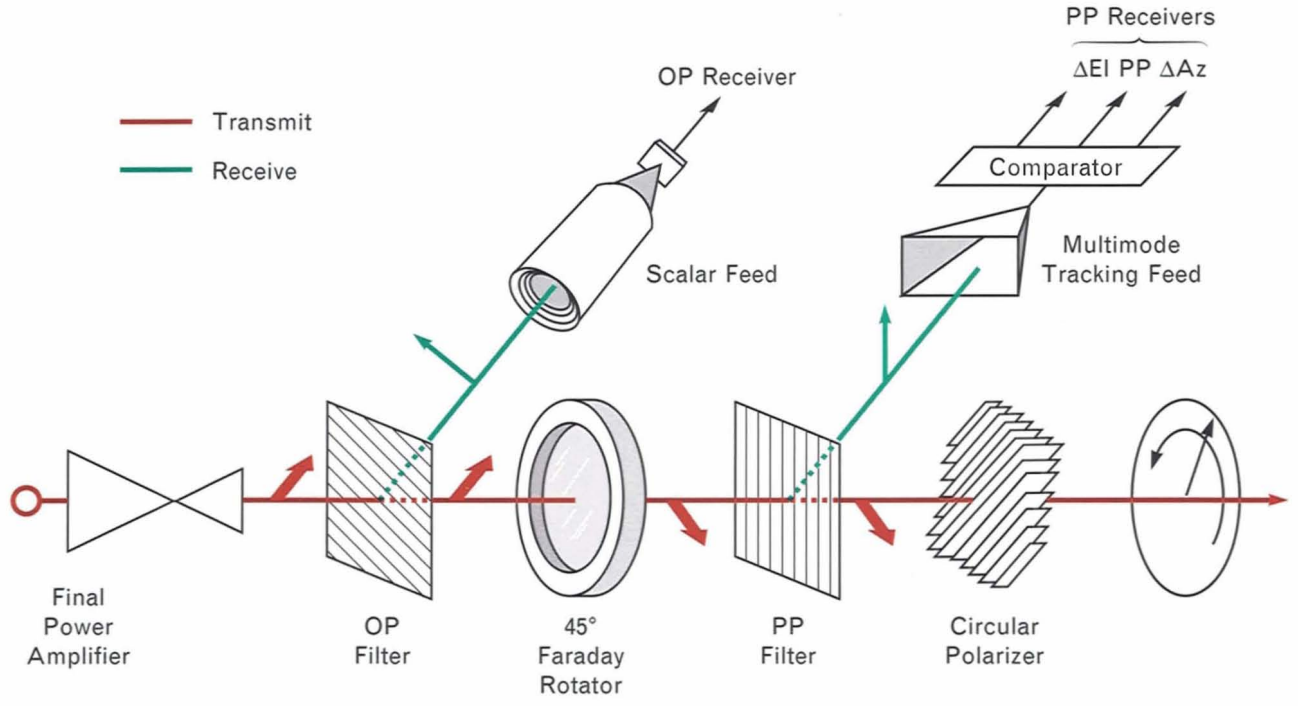

FIGURE 3. A diagram of the quasi-optical BWG system with the same functional requirements as the microwave system illustrated in Figure 2.

the same performance characteristics as the microwave system. A linearly polarized signal from the final power amplifier has a polarization perpendicular to the wires of the PP filter, and therefore passes through unaffected. The Faraday rotator rotates the polarization 45° to pass through the PP filter in a similar manner. The linear signal is transformed to circular polarization by the circular polarizer and then radiated. On reception, the preferred circular sense becomes linear (after the signal passes through the circular polarizer) and parallel to the wires of the PP filter, and is reflected to the PP receivers. The OP received signal similarly passes through the PP filter to be rotated 45° by the Faraday rotator (a nonreciprocal device) and is then tapped off by the OP filter to the OP receiver.

The principal advantages of the BWG system are reduced losses (spacial beams have no metallic walls), higher power-handling capability (power densities are typically less than –20 dB from conventional waveguide levels), and broader bandwidths (the reflectors are not independent of frequency as with conic sections based on ray optics, but 20% to 30% bandwidths are feasible).

Figure 4 shows the MMW Cassegrain antenna system. The transmitters and receivers are located in an enclosure—the RF Box—located behind the vertex of the main reflector. This RF Box is attached to the reflector structure; hence the system does not require rotary joints. The high-power microwave system and the receiver front ends are supported by a feed frame located forward of the vertex. The two frequencies are combined with a frequency-selective surface, which is simply a high-pass filter reflecting the 35-GHz signal in such a way that a virtual mirage of the feed is created at the Cassegrain focal point, coincident with the 95-GHz feed horn. We replaced the 35-GHz microwave system with a BWG, while retaining the frequency-selective surface and reserving space for a future 95-GHz BWG system.

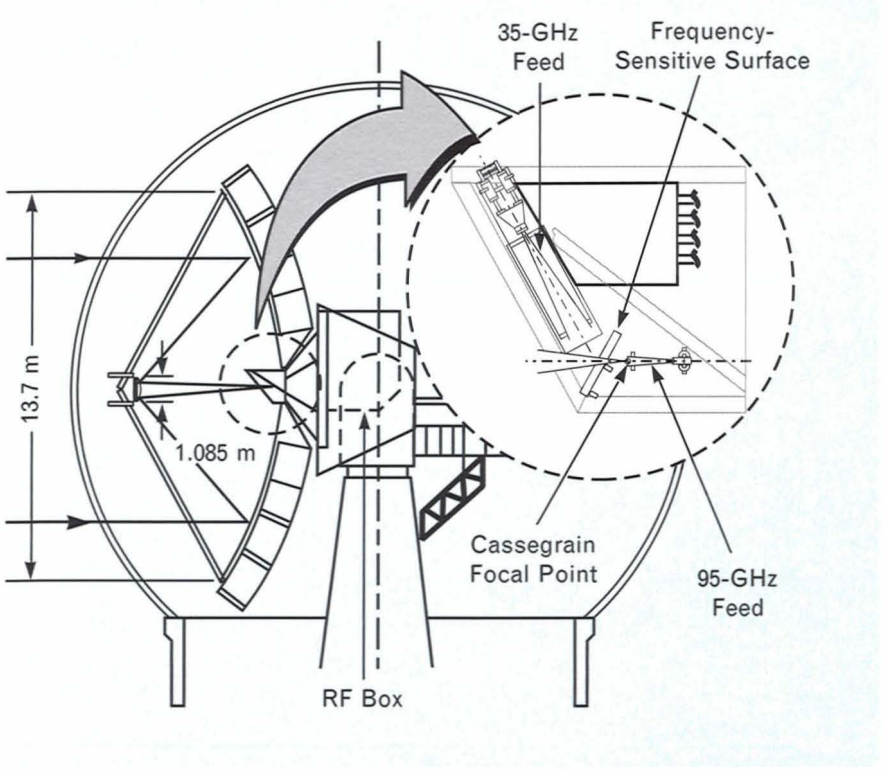

FIGURE 4. The MMW antenna system. The feed frame (shown in blowup) that formerly housed the microwave system was replaced with a new frame designed for the BWG. The frequency-sensitive surface was retained, and ample space was provided for a future 95-GHz BWG system.

The objective of the BWG modification is to increase the single-pulse sensitivity by 10 dB and provide for a future increase in system bandwidth from 1 to 2 GHz. Varian Associates, in a parallel program, developed a new traveling-wave tube that doubles the power output (to 50 kW) and bandwidth (to 2 GHz). The Lincoln Laboratory BWG program is divided into three phases: (1) replace the conventional feed and microwave system with the BWG (a 4-dB loss reduction), (2) replace the existing traveling-wave tube with the new Varian tube (a 3-dB power increase), and (3) parallel two of the new traveling wave tubes with a quasi-optical two-tube combiner (an additional 3 dB), for a total sensitivity enhancement of 10 dB. The BWG, including the two-tube combiner, has been installed and both of the new Varian tubes are in operation. Full-power output has been delayed, however, because of power-supply limitations.

After a brief introduction to Gaussian beam theory, we will describe in turn the design of the reflectors and quasi-optical components, the development of procedures for laser alignment, the results of assembly and testing, the installation of the BWG on the MMW antenna, and, finally, the evaluation of the system.

Gaussian Beams

Gaussian beam-mode theory has been extensively developed in the last two or three decades. The objective of the theory is to describe compact optical systems with a relatively small number of wavelengths in transverse extent; this number is too small to be described with classical techniques of ray optics. Numerous books and articles give complete descriptions of Gaussian mode theory [6, 7], which describes complete sets of orthogonal modes as a Gaussian envelope multiplied by Hermite polynomials (for Cartesian coordinates) or Laguerre polynomials (for polar coordinates). Higher-order Hermite-Gaussian modes are used for monopulse angle tracking, and higher-order Laguerre-Gaussian modes are generally associated with applications requiring circular symmetry, such as the analysis of scalar feed-horn distributions. Virtually all of our BWG component designs are based on the fundamental, or first order, Gaussian mode. The beam parameters for this mode are chosen to illuminate the MMW Cassegrain antenna efficiently, and this beam is then used to design the reflectors that periodically refocus the beam and the various quasi-optical components.

The fundamental Gaussian mode, which is illustrated in Figure 5, can be represented as a scalar field distribution as follows:

$$\Psi(x, y, z) = \left|\Psi(x, y, z)\right| e^{-ik\Delta(x,y,z)}, \qquad (1)$$

where

$$\left|\Psi(x, y, z)\right| = \frac{\omega_0}{\omega(z)} e^{-[r/\omega(z)]^2}$$

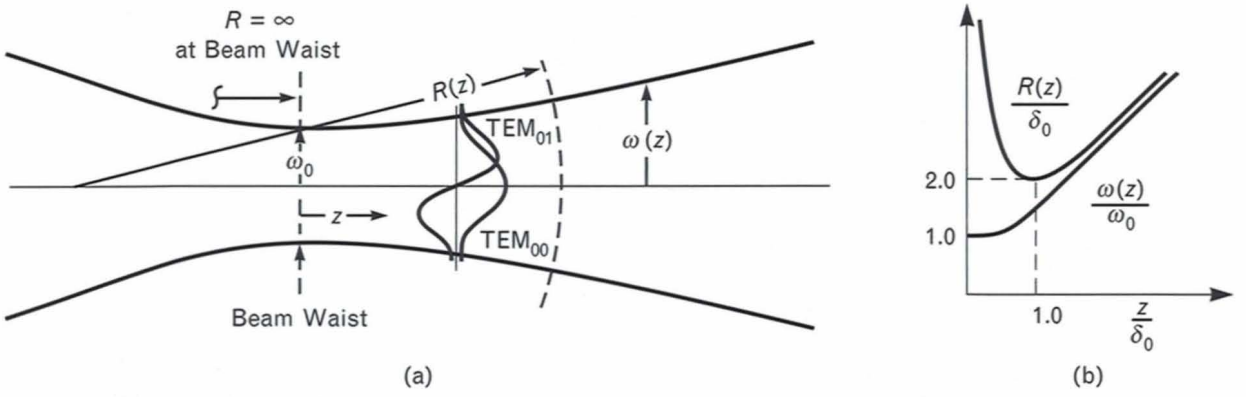

FIGURE 5. The geometry of Gaussian beams: (a) The minimum width of the beam occurs at the beam waist ($z = 0$) with a uniform phasefront ($R(0) = \infty$). The center of the spherical phasefronts varies with position along the z axis. The significant difference between modes is the amplitude distribution in a lateral plane. (b) Normalized characteristic parameters of Gaussian beams.

and

$$\Delta(x, y, z) = z + \frac{r^2}{2R(z)} - \frac{1}{k}\tan^{-1}\left(\frac{z}{\delta_0}\right).$$

The beam waist ω_0 is the $1/e$ radius at which the beam is at minimum width, z is the direction of propagation as measured from the beam waist, r is the radial distance from the beam axis (where $r^2 = x^2+y^2$), $\delta_0 = \pi\omega_0{}^2/\lambda$ is the confocal distance, or the boundary between near and far fields, and $k = 2\pi/\lambda$ is the wave number. The characteristic beam parameters are

$$\omega(z) = \omega_0\sqrt{1+\left(\frac{z}{\delta_0}\right)^2} \tag{2}$$

and

$$R(z) = z\left[1+\left(\frac{\delta_0}{z}\right)^2\right], \tag{3}$$

where $\omega(z)$ is the beamwidth and $R(z)$ is the radius of curvature of the approximate spherical phasefront. Equations 2 and 3 are valid for all higher-order modes as well as the fundamental mode. As a consequence, reflector designs based on these expressions, such as BWG layouts and iteration lengths, are valid for all Gaussian modes.

The Hermite-Gaussian modes are designated TEM_{mn}, where TEM_{00} is the fundamental mode and TEM_{01} is the principal mode used for angle tracking. The TEM_{01} mode differs from the fundamental mode principally by its amplitude distribution in a transverse plane (a z-dependent phase factor is of little significance). Gaussian beam modes are in sharp contrast to waveguide modes, with which we will be dealing in the design of the multimode feed, and which have widely differing cutoff frequencies and different propagation characteristics. For all Gaussian modes, the wavelength is free space throughout, from the beam waist to the far field. Consequently, BWG feed systems are completely free of distortion.

The Gaussian beam that optimizes the efficiency of the MMW antenna, which results in an approximate –12-dB edge illumination, has a beam waist ω_0 equal to 1.036 inches at 35 GHz. With the exception of the beam launchers, this fundamental-mode beam waist is used throughout the BWG system.

Reflector Design

A BWG system can be implemented with lenses or reflectors. The disadvantage of lenses is their low power-handling capability, which is due to the lack of suitable dielectric materials, as well as transmission loss, both dissipative and reflective. Reflectors can overcome these limitations, but they have some loss and cross-polarization generation because of the amplitude asymmetry of the required off-axis configuration. This deficiency with reflectors is tolerated by some applications, but it can be devastating for an angle-tracking radar in which we seek stable null depths less than –30 dB in the error channels. A symmetrical dual-reflector configuration has been developed that solves this problem.

The design of the reflectors is accomplished with Gaussian mode analysis, which is required with beams that are a relatively small number of wavelengths in transverse extent. A geometrical-optics analysis, which is based on ray tracing, is accurate when the beam dimensions are large in terms of wavelengths (i.e., as $\lambda \to 0$), and results in reflectors that are conic sections. The term *quasi-optical* applies in general to situations in which free-space transmission is involved but the underlying assumptions for ray tracing are not satisfied; hence a more rigorous diffraction analysis is required.

Figure 6 illustrates two Gaussian beams with different beam parameters being coupled by a reflecting surface. Our objective is to find the equation that describes the reflecting surface $z = f(x, y)$ in terms of the geometry l_1, l_2, and ϕ, and the characteristic input-beam and output-beam parameters $\omega(z)$ and $R(z)$ described by Equations 2 and 3. After reflection from the surface, the input beam has a common axis with the output beam. The power-transfer efficiency η with which energy is coupled between two coaxial fundamental Gaussian modes Ψ_1 and Ψ_2 with different beam-waist sizes and locations is given by

$$\eta = \frac{\left|\int_s \Psi_1\Psi_2^* ds\right|^2}{\int_s |\Psi_1|^2 ds \int_s |\Psi_2|^2 ds}, \tag{4}$$

where the asterisk indicates the complex conjugate [8]. The surface integrals are taken over the reflecting contour, and the fields must be expressed in the reflector coordinates (x, y, z). The power-transfer efficiency (where z_1 is negative to align propagating directions) can then be written as

$$\eta = \frac{\left| \int_s |\Psi_1||\Psi_2| e^{-ik(\Delta_1+\Delta_2)}\, ds \right|^2}{\int_s |\Psi_1|^2\, ds \int_s |\Psi_2|^2\, ds}. \tag{5}$$

Total power transfer (100% efficiency) is achieved if two conditions are met: the phase must be constant, and the amplitudes must be matched over the reflecting contour. We assume that the reflector is large enough to enclose essentially all the power in the beams. The phase term in Equation 5, which must be constant, is equal to the on-axis (or *boresight*) ray. Hence, from Equation 1,

$$\begin{aligned} &\Delta_1(x, y, z) + \Delta_2(x, y, z) \\ &\quad = \Delta_1(0, 0, 0) + \Delta_2(0, 0, 0) \\ &\quad = l_1 + l_2 - \frac{1}{k}\left(\tan^{-1} \frac{l_1}{\delta_{01}} + \tan^{-1} \frac{l_2}{\delta_{02}} \right). \end{aligned} \tag{6}$$

The phase functions defined in Equation 1 are transformed from individual beam coordinates (x_1, y_1, z_1) and (x_2, y_2, z_2) to reflector coordinates (x, y, z) with the following transformation:

$$\begin{aligned} x_1 &= x_2 = x \\ y_1 &= -y \cos\phi + z \sin\phi \\ z_1 &= -y \sin\phi - z \cos\phi + l_1 \\ y_2 &= -y \cos\phi - z \sin\phi \\ z_2 &= y \sin\phi - z \cos\phi + l_2 , \end{aligned}$$

where ϕ is the angle of incidence of the central ray at the reflector.

The amplitudes of the input and output beams are approximately matched at the reflector surface by setting $\omega_1(l_1)$ equal to $\omega_2(l_2)$, which leads to

$$\delta_{01}\left[1 + \left(\frac{l_1}{\delta_{01}}\right)^2\right] = \delta_{02}\left[1 + \left(\frac{l_2}{\delta_{02}}\right)^2\right]. \tag{7}$$

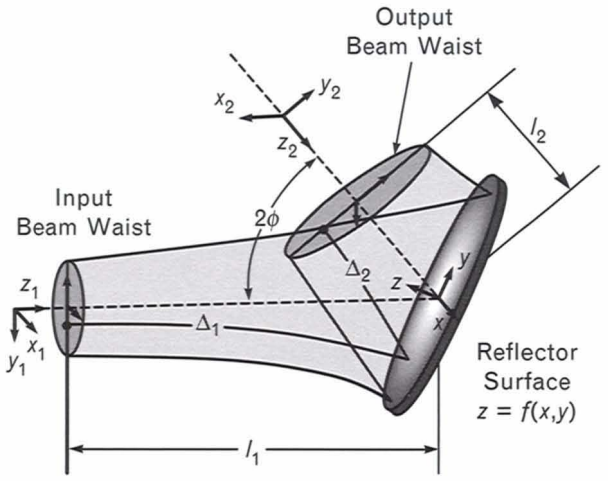

FIGURE 6. Two Gaussian beams with different beam parameters being coupled by a reflecting surface in an offset geometry. A single reflector has inherent cross-polarized components and amplitude unbalance that can be described with a Hermite-Gaussian TEM_{01} mode.

Satisfying this relationship between input-beam and output-beam parameters matches amplitudes exactly in the plane perpendicular to the bend, but only approximately in the plane of the bend (i.e., the plane of incidence). This mismatch, or space attenuation, is the source of higher-order mode and cross-polarization problems. Note that a BWG formed with lenses, because of its in-line geometry, does not generally experience amplitude mismatch or higher-order mode problems.

The equation describing the surface contour is found by using the coordinate transformations in Equation 6; the result is an unwieldy string of polynomials. A closed-form approximation of the surface contour is

$$z = \frac{\left(1 + ay \sin\phi\right)\left(x^2 + y^2 \cos^2\phi\right)}{\cos\phi\left\{b + cy \sin\phi + d\left[x^2 + \left(1 - 3\sin^2\phi\right)y^2\right]\right\}}, \tag{8}$$

where ϕ is the angle of incidence of the central ray at the reflector. The constants a, b, c, and d are expressed

in terms of the input-beam and output-beam parameters l_1, l_2, δ_{01}, δ_{02}, and λ. The beam parameters must satisfy Equation 7, which states the condition for approximate amplitude match at the reflector.

The above formulation is a scalar diffraction analysis that is also valid for paraxial ray optics. For example, the relation $l_1 >> \delta_{01}$ describes a Gaussian beam in the far field ($R(z_1) \rightarrow z_1$), which is equivalent to a point source located at $z_1 = 0$, and the relation $l_1 << \delta_{01}$ represents a plane wave at $z_1 = 0$. The relations are similar for l_2 and δ_{02}. Equation 8 describes an offset section of paraboloid with a point-source input ($l_1 >> \delta_{01}$) and a plane-wave output ($l_2 << \delta_{02}$); this equation also describes a section of an elliptic paraboloid with two point sources, as well as other conic sections used in ray-optics formulations. If either l_1 or l_2 is negative, Equation 8 describes a convex reflecting surface, e.g., a hyperboloid with ϕ equal to zero and two point sources.

More generally, when l_1 is comparable to δ_{01} or l_2 is comparable to δ_{02}, or both, we are in the Fresnel, or near field, of the aperture (we consider the beam waist to be a uniform phase aperture). The lateral dimensions are not large enough to view the beam as a plane wave; hence the center of the spherical phasefront varies for different points on an offset reflector, which requires a diffraction analysis. Most of the reflectors used in the MMW system are in this category. Unlike the ray-optics-based conic sections, which are independent of frequency, these reflectors have a slight frequency dependence that fortunately is of little practical significance. Bandwidths of 20% to 30% can easily be achieved. Working in the near field of a general aperture is an extremely complicated undertaking, but the Gaussian beam analysis avoids this problem.

The expression for the surface contour of the reflector described by Equation 8 is easily programmed for use with a computer-controlled milling machine. The Lincoln Laboratory machine shop fabricated the reflectors for the MMW BWG system and maintained surface tolerances less than 0.002 in rms.

Because of off-axis geometry, the curvature of a single reflector introduces a cross-polarized component, which is accompanied by coupling to a higher-order mode. The amplitude asymmetry in the plane of the bend (i.e., the amplitude mismatch between the input and output beams) gives rise to the higher-order mode. M.J. Gans has shown that a cross-polarized Hermite-Gaussian TEM_{01} mode accounts for both the cross-polarized fields and the amplitude asymmetry, or *space taper* [9]. He shows that the maximum cross-polarized field, relative to the copolarized field, is given by

$$C_m = \frac{2\omega(l)}{\sqrt{e}} K_\perp \sin\phi\,, \tag{9}$$

where $\omega(l)$ is the $1/e$ amplitude at the reflector, $K_\perp$ is the reflector curvature perpendicular to the plane of incidence, and ϕ is the angle of incidence. The peak cross-polarized signal occurs in the plane perpendicular to the plane of the bend with a null on-axis. If we set y equal to zero in Equation 8 and recognize that b is much greater than d, then

$$K_\perp = \frac{2}{b\cos\phi}$$

and

$$C_m = \frac{4\omega(l)}{b\sqrt{e}} \tan\phi\,, \tag{10}$$

where $\omega(l)$ refers to $\omega_1(l_1)$ of the input beam or $\omega_2(l_2)$ of the output beam, and $\omega_1(l_1)$ equals $\omega_2(l_2)$ for amplitude matching.

The ratio C_m is a measure of the level of undesired TEM_{01} mode generated by the reflector. The resulting loss, which is typically less than 0.1 dB, and cross-polarization, where the value of C_m is less than –20 dB, presents a serious problem for a monopulse radar. Coupling between the fundamental mode and the TEM_{01} mode (a mode with odd symmetry) disrupts the balance in the angle-error channels, which creates an unbalance that causes null shift and null fill with frequency (i.e., tracking jitter). The mode-coupling characteristics of offset reflectors cannot be tolerated in a BWG system designed for a precision angle-tracking radar. Our solution was to create a dual-reflector configuration—the *clamshell*—that achieves the high degree of mode purity required by the cancellation of the undesired higher-order mode generated by each reflector.

Figure 7 shows a symmetrical clamshell pair in

which the input and output beams and the two reflectors are identical. The reflector is designed by identifying an intermediate output beam waist in the plane bisecting the two reflectors; the parameters of the intermediate beam are readily found by using Equation 7, which gives the condition for matching amplitudes. If the axial separation d between reflectors is much less than δ_0^2, which is an easily satisfied condition, then the single undesired TEM_{01} mode generated at each reflector cancels the other. The dominant TEM_{00} mode as well as the angle-tracking modes TEM_{01} and TEM_{03} are refocused by the clamshell without distortion or cross-polarization generation. Measurements show that the cross-polarization for a symmetrical pair is less than –40 dB for any orientation of the input polarization. Reflectors are sized to capture the fundamental mode down to at least –35 dB to assure the purity of the beam that is reproduced with each iteration.

The beam launcher uses a nonsymmetrical clamshell, which transforms an input beam to an output beam with a different beam waist. Here the reflector curvatures differ, which leads to incomplete cancellation of the offending TEM_{01} modes. Each reflector has an angle of incidence ϕ equal to $\pi/4 - \theta/4$, where θ is the angle between input and output beams. For the single reflector, ϕ is equal to $\theta/2$. From Equation 10, each of the dual reflectors has approximately half the cross-polarized component of a single reflector for the important case where θ equals $\pi/2$. This fact further reduces the net cross-polarized component for the nonsymmetrical clamshell, where cancellation is incomplete.

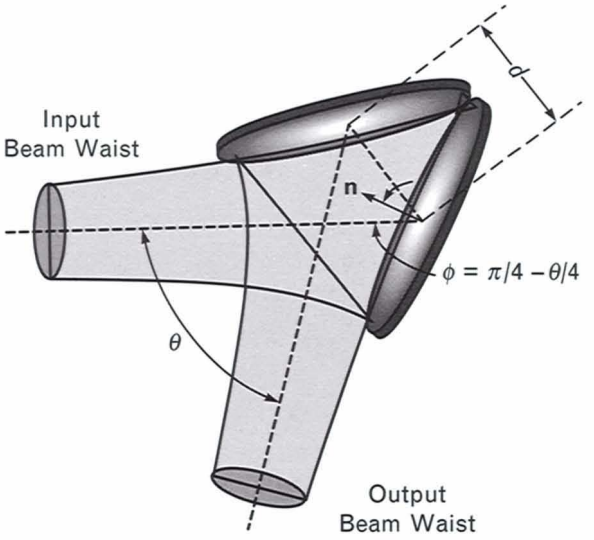

FIGURE 7. Symmetrical clamshell reflectors. The reflector is designed by identifying an intermediate output beam waist in the plane bisecting the two reflectors. A high level of mode purity is achieved by cancellation of the effects of unbalance or, equivalently, the cancellation of the TEM_{01} modes generated at each surface.

Beam Launcher

A scalar, or *corrugated*, feed horn is well suited as a transition from a waveguide to a Gaussian beam [10]. It has a circularly symmetric aperture distribution that is free of cross-polarized components, and consequently it makes a good approximation to a Gaussian beam. The aperture distribution is given by

$$E(r) = J_0\left(2.405\frac{r}{a}\right)e^{-\frac{\pi r^2}{\lambda R_h}} \qquad 0 \le r \le a\,,$$

where a is the radius of the horn aperture, J_0 is the zero-order Bessel function, and R_h is the radius of curvature (centered at the horn vertex) of the phase front at the aperture. Figure 8 defines the coupling of the scalar feed horn to the Gaussian beam. Figure 8(a) shows the geometry of the scalar feed. R.J. Wylde expands this aperture field into an orthogonal set of Gaussian-Laguerre modes and shows that approximately 98% of the power radiated by the horn is in the fundamental Gaussian mode if a is equal to $1.554\,\omega(z_1)$ [11]. This fact relates the size of the horn aperture to the width $\omega(z_1)$ of the Gaussian beam at the aperture, where the beam waist is a distance z_1 behind the aperture.

By using Equations 2 and 3, and by setting R_h (the radius of phase curvature at the horn aperture) equal to R (the radius of curvature of the Gaussian beam), we have

$$\omega(z_1) = \frac{a}{1.554} = \omega_0\sqrt{1 + \left(\frac{z_1}{\delta_0}\right)^2} \qquad (11)$$

and

$$R = R_h = z_1\left[1 + \left(\frac{\delta_0}{z_1}\right)^2\right]. \qquad (12)$$

Figure 8(b) shows a plot of the relationships in Equations 11 and 12. If we require a Gaussian beam of waist ω_0 located at $z = 0$, then we have an infinite set of scalar feeds from which to choose. The minimum-length horn corresponds to the minimum value of R for the Gaussian beam (this value occurs when z_1/δ_0 equals 1); at this point R_h equals $2\delta_0$ and a equals $1.554\sqrt{2}\,\omega_0$. A horn of infinite length (i.e., uniform phase aperture) has an aperture with radius a equal to $1.554\omega_0$. For a given horn defined by R_h and a, we again utilize Equations 2 and 3 to express ω_0 and z_1 in terms of the horn parameters R_h (equal to R) and a (equal to $\omega(z_1)/1.554$):

$$\omega_0 = \frac{\omega(z_1)}{\sqrt{1 + \left(\frac{\pi\omega^2(z_1)}{\lambda R_h}\right)^2}} \qquad (13)$$

and

$$z_1 = \frac{R_h}{1 + \left(\frac{\lambda R_h}{\pi\omega^2(z_1)}\right)^2}. \qquad (14)$$

These equations determine the parameters of the Gaussian beam generated by the horn. The phase center for the horn is at the beam waist, which is a distance z_1 behind the aperture plane.

Figure 9(a) shows the configuration of the beam launcher. A relatively short horn was chosen for convenience, and the output beam waist is well separated (approximately 11 in) from reflector B to make the beam launcher compatible with the BWG layout. The short horn requires the clamshell reflectors to function as a beam converter. In other words, the input beam waist (ω_{01} = 0.535 in) is converted to an output beam waist (ω_{02} = 1.036 in), which is the required width to illuminate the MMW antenna efficiently. This conversion requires an asymmetrical clamshell pair. At the output beam waist, the beam

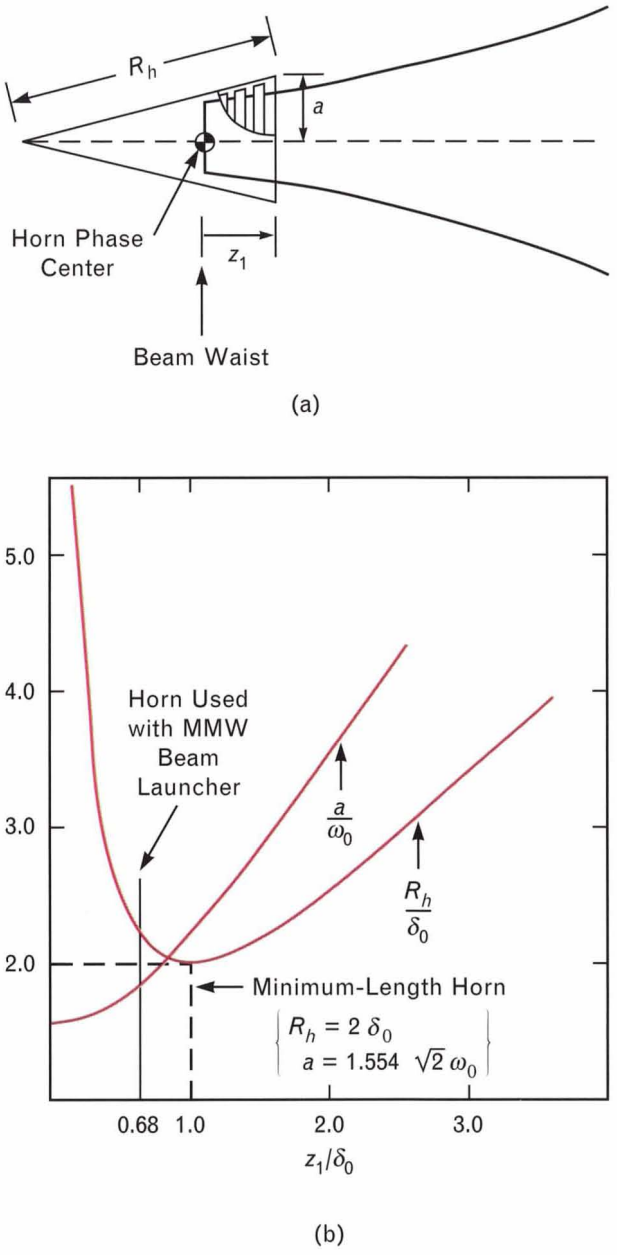

FIGURE 8. Scalar, or corrugated, horn coupling to a Gaussian beam: (a) The geometry of the scalar horn. (b) The design curves show the relation between the scalar horn and the fundamental Gaussian mode excited. Any one of an infinite set of horns couples to a specific Gaussian beam defined by z_1 and δ_0.

launcher is equivalent to an image scalar feed with R_h equal to ∞ (a uniform phase aperture) and an aperture radius a equal to $1.554\omega_{02}$. The reflectors are designed by identifying a beam waist in the bisecting

plane, as previously described, which is used to design both reflectors. Reflector A has an input beam determined by Equations 13 and 14 from the feed-horn dimensions. The asymmetrical clamshell provides flexibility in the design of the beam launcher, which is significant when space is at a premium. Reducing the input beam waist by a factor of 2, for example, reduces the scalar horn length by a factor of 4. The scalar feed design is from D.C. Weikle [12].

Figure 9(b) shows the measured *E*-plane and *H*-plane patterns of the beam launcher, compared to the theoretical patterns of the image scalar feed. The measured phase center of these patterns is at the output beam waist as expected. From Equation 9, the maximum cross-polarized component C_m from reflector A is 0.049 (–26.2 dB) and from reflector B is 0.022 (–33.7 dB). The cancellation is incomplete because of the asymmetry of the reflectors. The uncancelled cross-polarized component (equal to –31.5 dB), which represents the net amount of undesired TEM_{01} mode generated, is in excellent agreement with the measured level shown in the figure. The measured cross-polarization is in the plane normal to the plane of the bend. Wylde has shown that the second-order Gaussian-Laguerre mode accounts for the 2% of the power not included in the fundamental mode [11]. Other higher-order modes are insignificant. The second-order mode is in phase with the fundamental mode at the horn aperture, not at the beam waist (where $z_1 = 0$). Consequently, a differential phase shift of approximately 52° appears at the output beam waist, which accounts for the null fill-in observed between main lobe and sidelobes.

The Quasi-Optical Circulator

The limited power-handling capability of the standard waveguide differential phase-shift circulator was a major obstacle to increasing the MMW system power level. All four of the waveguide circulator units used in the microwave system (see Figure 2) failed at average power levels of approximately 600 W, which is consistent with the state-of-the-art power-handling data presented by G.P. Rodrigue [13]. The quasi-optical circulator, which was first described by G.F. Dionne et al. [14], offers performance characteristics, such as bandwidth, insertion loss, and isolation, that are significantly better than the waveguide circulator. A fundamental advantage for the quasi-optical circulator, and more generally for all quasi-optical components, is the dramatic reduction in the power density encountered. The on-axis power density for the beam size chosen (ω_0 = 1.036 in) is down 23 dB from the level in a WR-28 waveguide carrying the same total power.

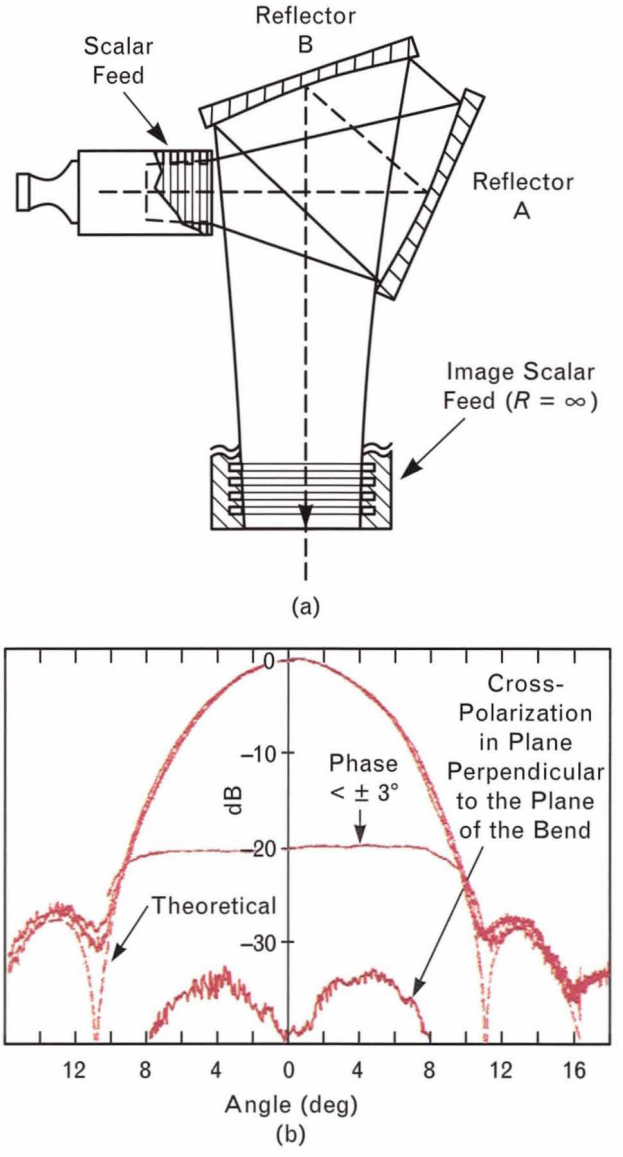

FIGURE 9. (a) The beam launcher is a scalar feed with an asymmetrical clamshell that behaves as if it were a larger scalar feed (the *image* feed) with a uniform phase aperture at the output beam waist. (b) Measured patterns compared to the theoretical image-feed patterns.

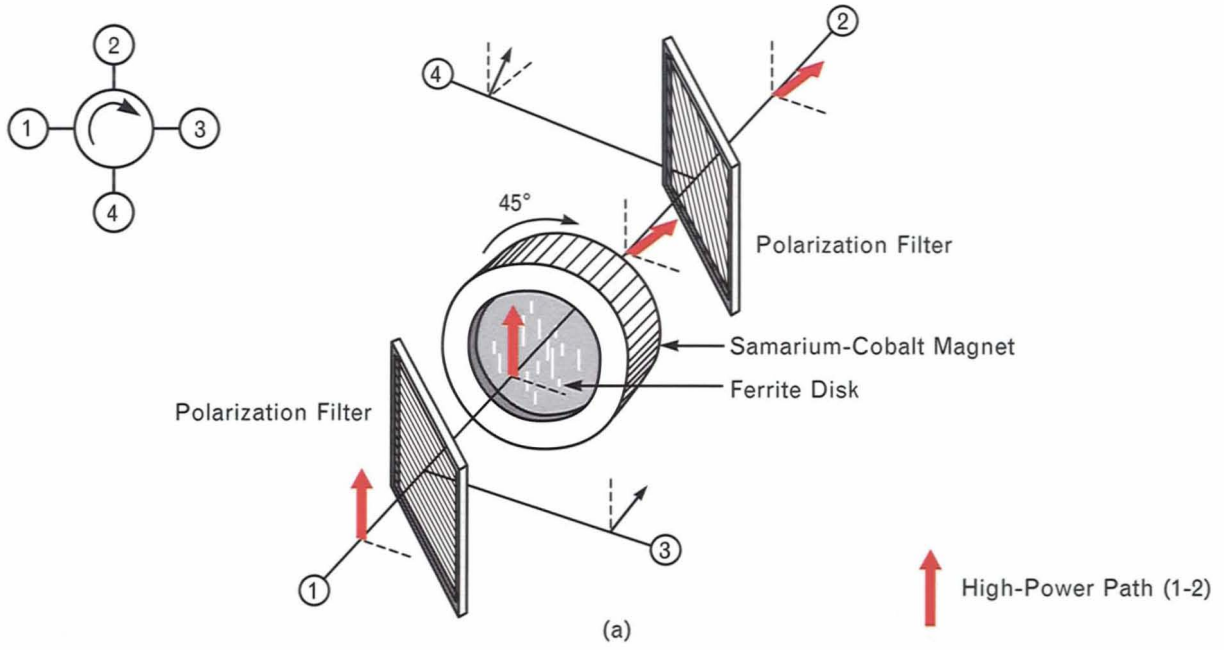

FIGURE 10. (a) The four-port quasi-optical circulator, composed of two properly oriented polarization filters and a Faraday rotator. (b) A photograph of the Faraday rotator.

Figure 10(a) illustrates the four-port quasi-optical Faraday rotation circulator, which is analogous to the waveguide Faraday rotation circulator originally described by B. Lax and K. Button [15]. The parallel wire grids on each side of the Faraday rotator are set at 45° to the axis. These polarization filters pass a signal with its polarization perpendicular to the wires and reflect the parallel polarization. The power-transfer paths are ports 1 to 2, ports 2 to 3, and so on, as indicated in the schematic for the circulator. The important performance characteristics for our application are insertion loss from ports 1 to 2 (the high-power path) and from ports 2 to 3 (the OP receiver path), and the isolation between port 1 (the higher-power input) and port 3 (the OP receiver). Port 4 is effectively terminated. The PP receive signal appears as an orthogonal input to port 2, which is reflected in the opposite direction from port 4 without passing through the circulator. The polarization of the high-power transmit signal is always normal to the wire grids of the polarization filters. The other configuration, with the high-power signal parallel to the wire grid, would restrict power-handling capability.

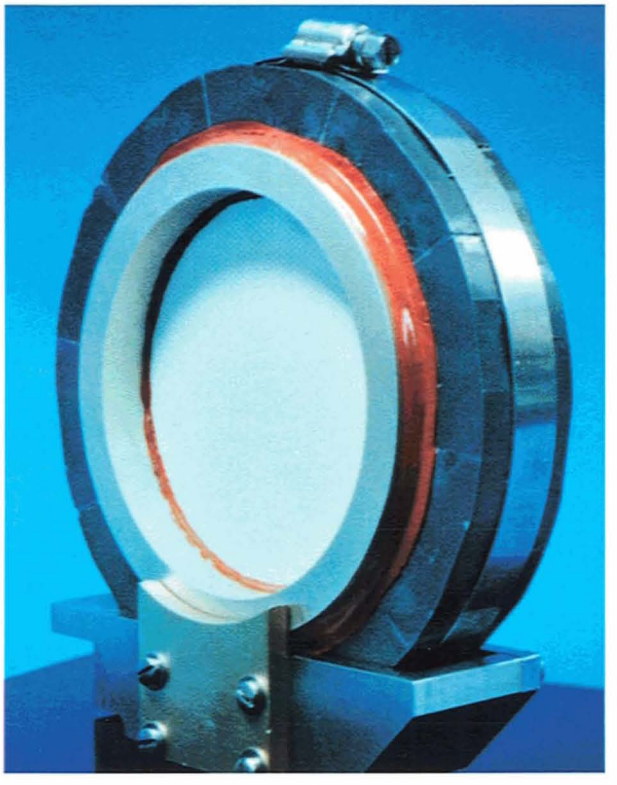

(b)

The heart of the quasi-optical circulator illustrated in Figure 10(a) is the nonreciprocal 45° Faraday rotator shown in Figure 10(b). This rotator consists of a toroidal samarium-cobalt permanent magnet that pro-

vides the axial magnetic field and houses the ferrite disk. The ferrite material is an yttrium-iron garnet (the magnetization $4\pi M_s \cong 800$ Gauss) provided by Trans Tech Inc. in Adamstown, Md. The axial field of the toroidal permanent magnet is greater than 1000 Gauss, which is sufficient to overcome the demagnetizing field of the ferrite disk. Slight off-axis variations of the external magnetic field are of no consequence as long as the ferrite material is saturated throughout. The Faraday rotator is placed at a beam waist, and the 4-in diameter of the ferrite disk is sufficient to encompass the Gaussian beam down to –35 dB.

The theory of gyromagnetic Faraday rotation is well known [13]. Suffice it here to note that a linearly polarized plane wave passing through the ferrite disk has its polarization rotated by an angle

$$\theta = \frac{\pi\sqrt{\varepsilon_f}}{c}\,\gamma(4\pi M_s)t\,, \qquad (15)$$

where ε_f is the dielectric constant of the ferrite material, γ is the gyromagnetic constant, $4\pi M_s$ is the magnetization, t is the thickness of the ferrite disk, and c is the velocity of light. This approximation is valid if the ferromagnetic resonance frequency is less than the operating frequency (the *below-resonance* condition), and if $\gamma(4\pi M_s)$ is also less than the operating frequency. A design with high-magnetization ferrite requires a heavier magnet but reduces the thickness and therefore the loss of the ferrite disk. A thinner ferrite disk also eases the heat removal problem. The polarization rotation given by Equation 15 is independent of frequency.

The ferrite material has low loss (the loss tangent is approximately 0.0001), but unfortunately it also has low thermal conductivity. Consequently, the high-power design problem is largely a problem of heat removal. The approach we took was to divide the disk in two and insert an aluminum-nitride (ALN) heat sink between the halves, as indicated in Figure 11(a). The ALN, which is a half-wavelength thick for impedance matching, is a low-loss dielectric with moderately high thermal conductivity. The dual-disk design reduces the heat generated in each ferrite disk by half, and also reduces the average heat-flow path to the disk surface by half. To first order, the dual-disk

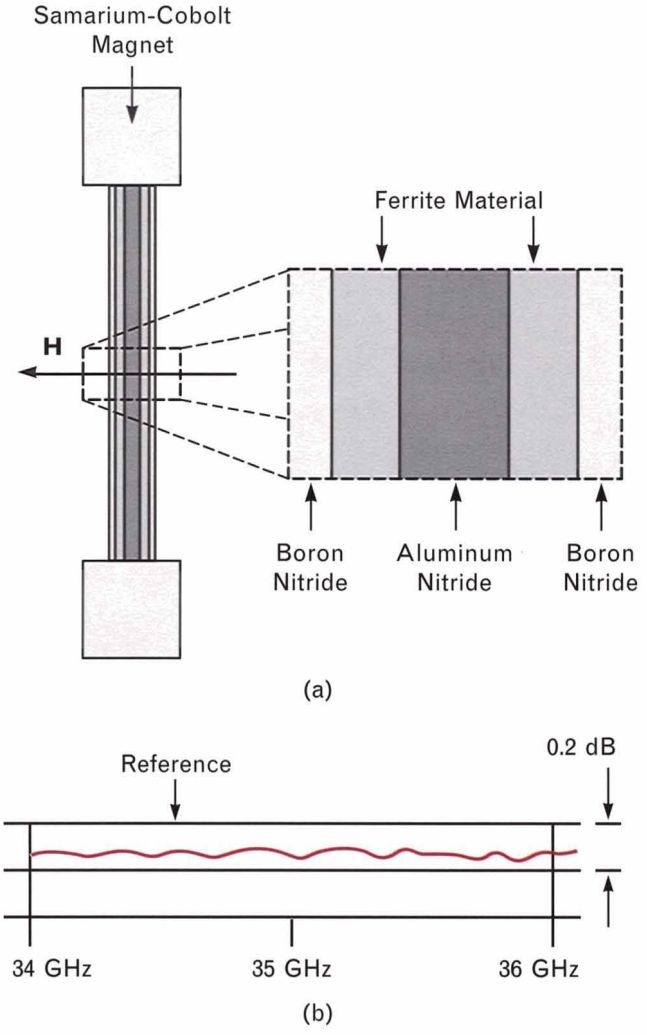

FIGURE 11. (a) Cross section of the dual-ferrite-disk Faraday rotator design, which has a half-wavelength aluminum-nitride heat sink inserted between the ferrite halves. (b) Measured insertion loss of the Faraday rotator. The only cooling in the BWG system is an air flow directed at the boron-nitride outer faces of the rotator.

design quadruples the average power-handling capability of the rotator. Matching the outer ferrite faces is accomplished with a quarter-wave boron-nitride matching plate, which also has good thermal conductivity. These plates are perforated with many small holes to reduce the effective dielectric constant to the required value of 3.8. Impedance matching at each face of the ferrite material eliminates multiple reflections, or standing waves, in the ferrite material. These reflections, if present, would result in more loss and

frequency-dependent components of rotation. Another consideration for a high-power device is the temperature dependence of the ferrite magnetization. From Equation 15 we know that polarization rotation is proportional to $4\pi M_s$; hence a material with a flat $4\pi M_s$ versus temperature is desirable. The material chosen permits a temperature rise of 100°C without appreciable change in polarization rotation. The only cooling employed is an air flow directed on the boron-nitride faces.

High peak power in ferrite materials can trigger a nonlinear magnetic loss mechanism. The onset of this loss is proportional to $(\Delta H_k)^2$, where ΔH_k is the spin-wave line width of the material. High-power experiments performed at the Varian test facility with a low-ΔH_k (approximately 1.5 Oe) ferrite material showed no evidence of nonlinear loss with peak power levels to 23 kW. The ferrite used in the Faraday rotator has a ΔH_k of approximately 6 Oe. By extrapolation, the minimum level at which peak-power problems might occur is 350 kW, which is well beyond our capabilities. Figure 11(b) shows the measured transmission loss of the Faraday rotator; the observed loss of 0.15 dB includes the effects of reflections, diffraction, and dissipative losses. Almost half of this loss occurs in the ALN heat sink.

Figure 12 is a photograph of the completed quasi-optical circulator mounted in the system. The Faraday rotator is positioned at a beam waist. The polarization filters—the wire grids—on each side of the Faraday rotator tap off the PP and OP receive signals. The wire-grid filters are each attached to a rectangular aluminum frame that slides out of the holder for easy replacement. At the left in the photograph of the circulator is a plexiglass frame over which is stretched a thin (less than 0.001 in) dielectric membrane. This membrane is a quasi-optical directional coupler that monitors the peak power radiated.

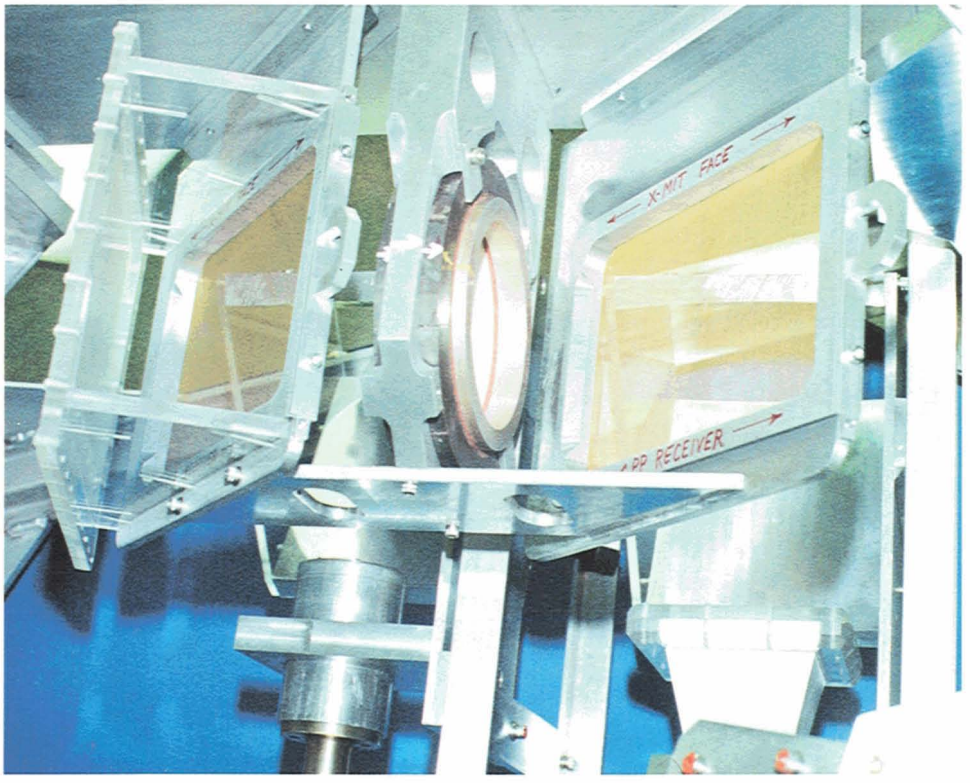

FIGURE 12. The completed quasi-optical circulator in the BWG system. The Faraday rotator is at a beam waist, and each of the two polarization filters is mounted at an angle of 45° to the beam path. A membrane supported by a plexiglass holder at the left is a –40-db quasi-optical coupler that functions as the peak-power monitor for the system.

The Multimode Feed

High efficiency and good monopulse angle-tracking characteristics can be achieved in a Cassegrain system with the use of a multimode feed [16]. The high efficiency achieved by the introduction of higher-order beam-shaping modes is as good as the best pencil-beam feeds (e.g., a scalar feed, or the fundamental Gaussian mode). The best comparative measure of Cassegrain feeds is the product of the spillover efficiency η_{sp}, which is principally a measure of the energy lost in sidelobes, and the aperture taper efficiency η_{ap}. Other efficiency factors that account for blockage, tolerances, and phase errors are, to first order, the same for all feeds. Surprisingly, the optimized product $\eta_{sp} \times \eta_{ap}$ is exactly 81.4% for both the multimode feed and the fundamental Gaussian mode.

The multimode tracking feed for a conventional microwave system, as illustrated in Figure 2, must be a dual-polarized, high-power design. The BWG system configuration, as illustrated in Figure 3, separates transmit and receive paths to relax the requirements on the multimode feed, which then becomes a linearly polarized, low-power design. This simplification leads to improved efficiency and bandwidth. In addition, the cross-polarized coupling between difference channels (commonly referred to as *x-pol; x-talk*), which is a common problem with dual-polarized feeds (it creates angle-tracking problems when off-axis targets have strong depolarized returns), is completely eliminated.

Beam shaping in a pyramidal horn is accomplished by adding to the dominant TE_{10} mode the proper amount of TE_{12} and TM_{12} modes. These two additional modes, which are a degenerate pair, are designated the LSE_{12} (longitudinal section electric) mode. The higher-order modes are required to be in phase with the TE_{10} mode at the aperture. The efficiency is optimized with negligible energy loss in the sidelobes when the ratio LSE_{12}/TE_{10} is equal to 0.67.

The design procedure, which follows the work of S.B. Cohn, uses abrupt flare changes at one or more points along the axis of the horn to generate the LSE_{12} mode [17]. The ratio of mode amplitudes immediately after a flare change is given by

$$\frac{LSE_{12}}{TE_{10}} \cong j\frac{2a}{3\lambda}(\theta_1 - \theta_2),$$

where a/λ is the height of the horn in wavelengths at the flare break and $\theta_1 - \theta_2$ is the angular differential. Note that the LSE_{12} is generated in phase quadrature with the TE_{10}. When $\theta_1 - \theta_2$ is less than zero, the length of the horn between the flare break and the aperture must have a differential phase shift of $\pi/2$ for the modes to be in phase at the aperture. Similarly, when $\theta_1 - \theta_2$ is greater than zero, a differential phase shift of $3\pi/2$ is required.

Figure 13 shows the 35-GHz multimode horn design. The differential phase shift from the first flare break to the aperture is $3\pi/2$ and from the second flare break to the aperture is $\pi/2$. The short section (0.766 in) between the flare breaks suppresses the relatively small amount of the undesired LSE_{14} generated. Suppression is accomplished by adjusting the length of this section for a phase reversal, which cancels the LSE_{14} component without significantly affecting the LSE_{12} component. The output section of the horn consists of four reduced-width rectangular waveguides that are the inputs to the waveguide comparator. The reduced width of this section eliminates the TE_{30} mode at this junction. The only modes that can propagate at this point are the dominant (TE_{10}) mode and the angle-tracking modes (TE_{20} and LSE_{11}) in the two orthogonal planes. Finally, a dielectric lens is used to create a uniform phasefront at the horn aperture. The lens is a simple thin lens (i.e., a phase transformer that has negligible effect on amplitude distribution); its focal length is equal to the extended slant length of the final flare section. Matching is achieved on both surfaces of the lens by densely spaced grooves cut into the lens material (rexolite) to simulate quarter-wave matching sections. Figure 14 shows the completed horn assembled with the correcting lens and the waveguide comparator.

The multimode feed is not, as is usually the case, positioned at the Cassegrain focal point. Figure 15 shows the configuration of the PP receive path. The linearly polarized signal from the PP filter (which is the circularly polarized PP signal after passing through the polarizer) is focused to a beam waist at the horn aperture. The transformation from Gaussian modes

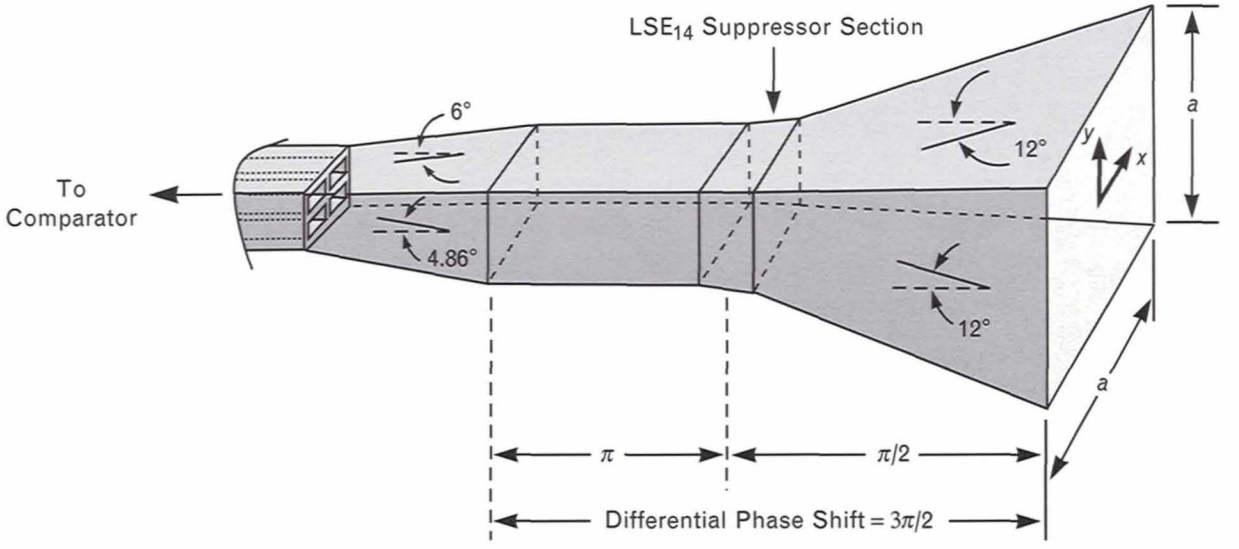

FIGURE 13. The geometry of the 35-GHz multimode angle-tracking horn. The junction with the four rectangular guides propagates only the dominant TE_{10} mode and the tracking modes TE_{20} and LSE_{11}. A dielectric phase-correcting lens is placed at the horn aperture.

to waveguide modes occurs in the horn-aperture plane. The fundamental Gaussian mode (TEM_{00}) couples to the TE_{10} and LSE_{12} waveguide modes, and the Gaussian TEM_{01} mode and a lesser amount of TEM_{03} couple to the waveguide tracking modes, which are the TE_{20} and the LSE_{11} for the two orthogonal planes.

Coupling between the horn and Gaussian beam can be determined by rewriting Equation 4. The

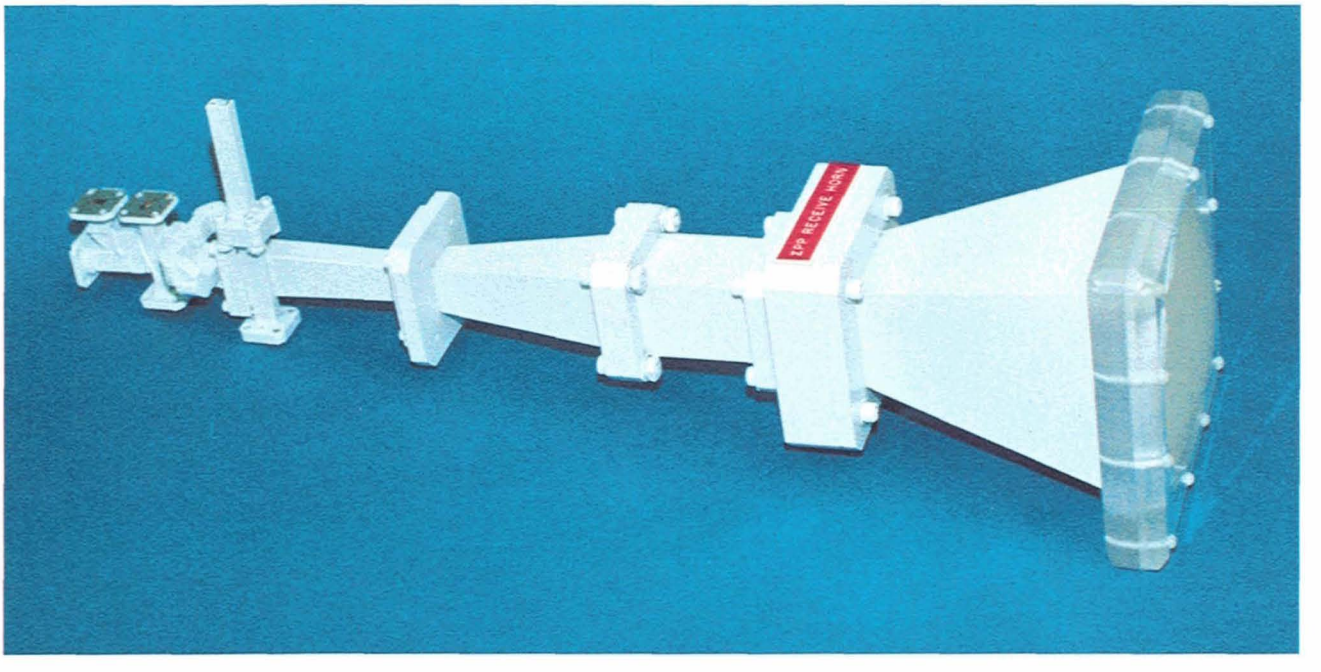

FIGURE 14. The 35-GHz multimode angle-tracking horn with correcting lens and waveguide comparator.

power-transmission efficiency η at a plane surface, which we take as the horn aperture, where both distributions have uniform phase and matched polarizations, is

$$\eta = \frac{\left| \int_{s_1} \Psi_1 \Psi_2^{*} \, ds_1 \right|^2}{\int_{s_1} |\Psi_1|^2 \, ds_1 \int_{s_2} |\Psi_2|^2 \, ds_2}, \qquad (16)$$

where Ψ_1 is the horn-aperture distribution and Ψ_2 represents the fundamental Gaussian mode. These quantities can be written as

$$\Psi_1 = \cos\frac{\pi x}{a}\left(1 + \frac{\mathrm{LSE}_{12}}{\mathrm{TE}_{10}} \cos\frac{2\pi y}{a}\right)$$

and

$$\Psi_2 = e^{-\left(x^2+y^2\right)/\omega_0^2},$$

where x and y are the coordinates of the horn aperture. The surface s_1 in Equation 16 is the horn aperture (which is a square of size $a \times a$), and the surface s_2 is the infinite plane associated with the Gaussian mode. Evaluating Equation 16 with $\mathrm{LSE}_{12}/\mathrm{TE}_{10}$ equal to 0.67 yields a peak efficiency $\eta_{\max}$ of 98.5% for a/ω_0 equal to 2.90. This result establishes the relationship between the width a of the horn aperture and the beam-waist radius ω_0 chosen to illuminate the MMW Cassegrain geometry efficiently.

Figure 16(a) shows the measured patterns of the multimode horn, and Figure 16(b) shows the mea-

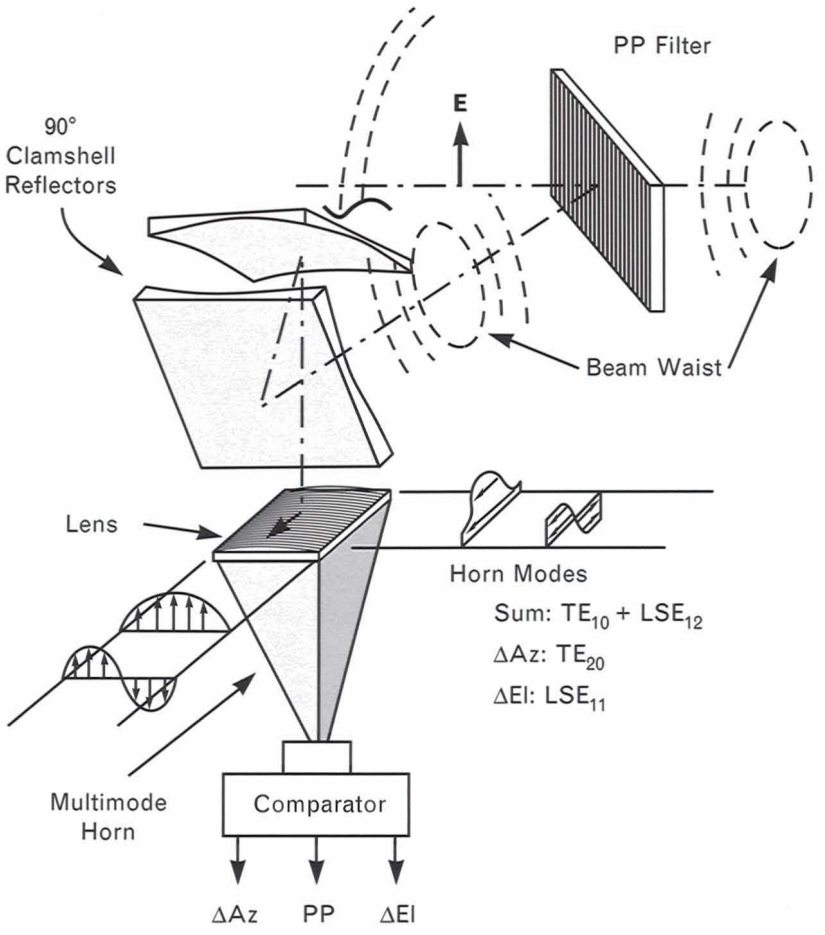

FIGURE 15. The configuration of the principal-polarization (PP) receive path. The transformation from the Gaussian modes (TEM_{00}, TEM_{01}, and TEM_{03}) to the waveguide modes (TE_{10}, LSE_{12}, TE_{20}, and LSE_{11}) occurs at the horn aperture.

sured patterns with the horn installed in the BWG system. The *E*-plane and *H*-plane patterns of the horn have equal beamwidths with sidelobes less than –23 dB. Also shown in Figure 16(a) are the difference patterns for the TE_{20} and LSE_{11} tracking modes. Figure 16(b) presents the completed BWG PP receive primary patterns. The balance in the difference patterns, which is required for good null depth in the secondary, is particularly good. The difference mode corresponding to the LSE_{11} waveguide mode in Figure 16(a) contains both the Gaussian TEM_{01} and TEM_{03} modes. These modes maintain their relative amplitude and phase relationships quite well over the band, because of the nondispersive propagation characteristics of all Gaussian modes.

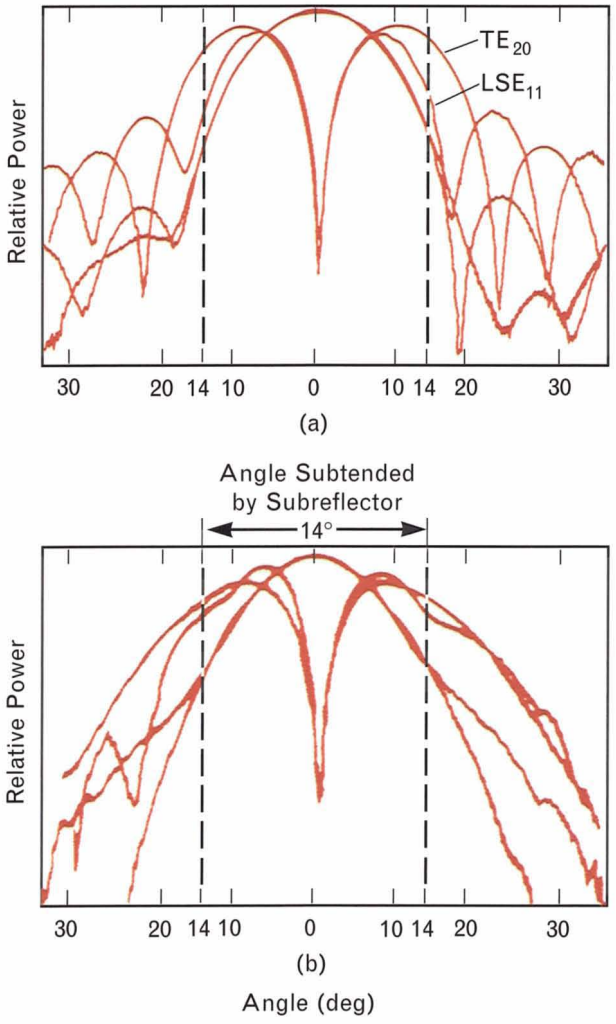

FIGURE 16. (a) Principal plane patterns of the multimode feed, and (b) principal plane patterns after the multimode feed is installed in the BWG system. These patterns illustrate the conversion from Gaussian to waveguide modes. The angle subtended by the subreflector is 14°.

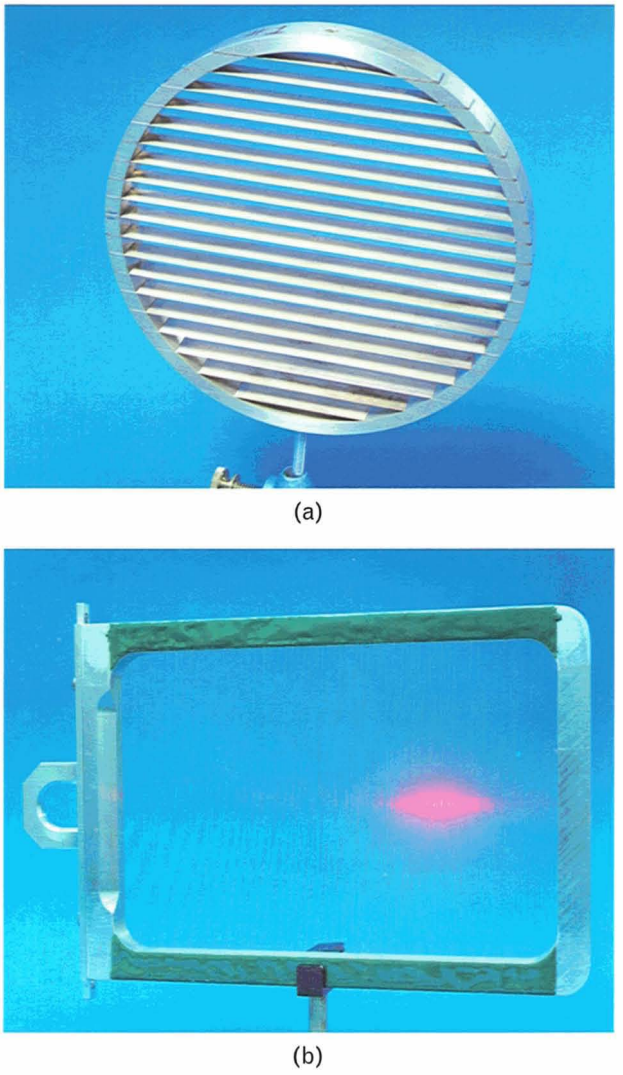

FIGURE 17. Quasi-optical components: (a) the Venetian-blind circular polarizer and (b) the parallel-wire-grid polarization filter.

Circular Polarizer

The circular polarizer, which is shown in Figure 17(a), is made up of parallel conducting strips similar in appearance to an open Venetian blind. The device is positioned at a beam waist with the strips oriented 45° to the incident linearly polarized signal; this orientation results in equal components perpendicular and parallel to the strips. The perpendicular component passes through with a free-space wavelength, and

the parallel component passes through with a wavelength equal to a TE_{10} mode in a rectangular guide of width equal to the separation between the strips. The depth of the strips is adjusted for a differential phase shift of 90° between the orthogonal components, which results in a circularly polarized output. This polarizer is not a particularly broadband device, but for the MMW bandwidth the increased axial ratio at the band edges is less than ± 0.7 dB.

Polarization Filters

The microwave orthogonal-mode transducer is a device that combines two orthogonally polarized components into a common path or, conversely, separates orthogonal components. The quasi-optical equivalent is the polarization filter, which is simple to fabricate and can handle high power over octive bandwidths with negligible losses. The device is simply a grid of conducting wires that presents a shunt inductance to the polarization parallel to the wires. The theory of these devices is described elsewhere [18]. With the proper diameter and spacing of the wires, the reflection coefficient for the parallel polarization is essentially unity (approximately 0.995), and the transmis-

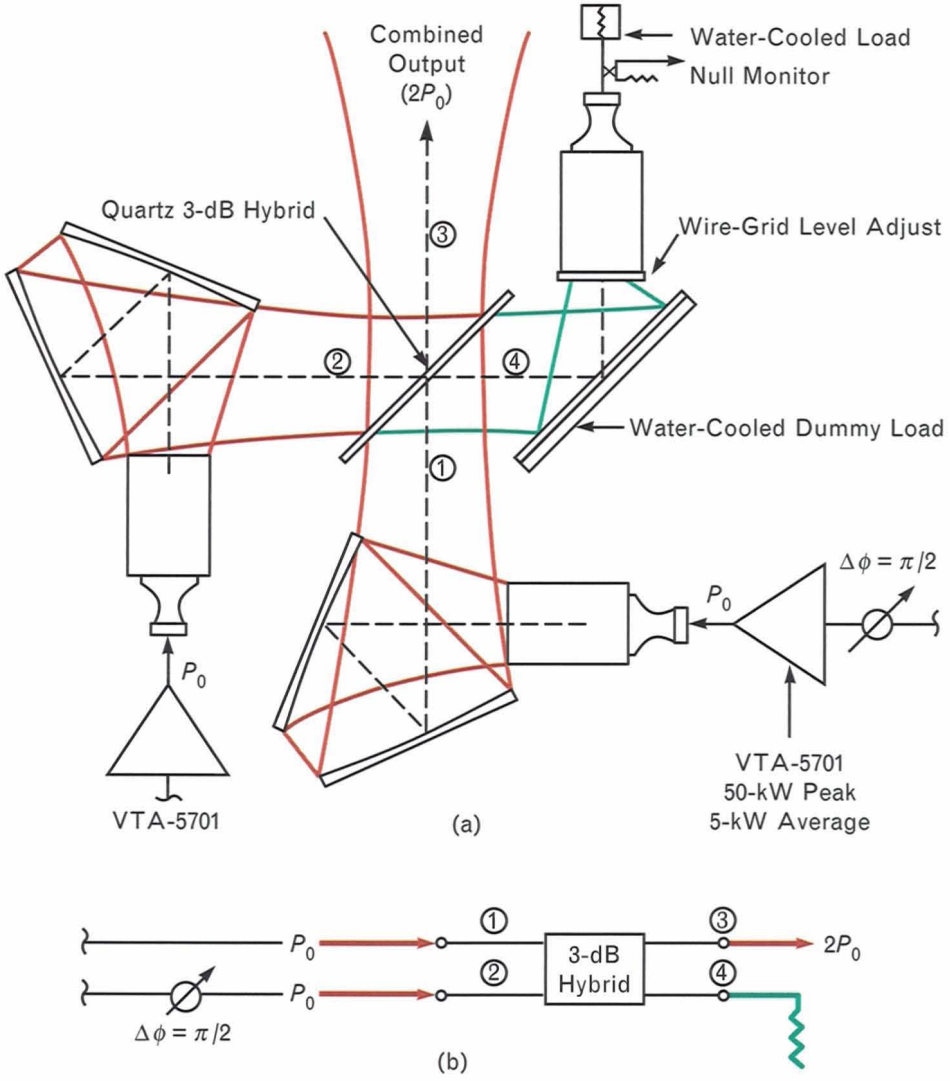

FIGURE 18. (a) Diagram of a quasi-optical two-tube combiner using two beam launchers; (b) the equivalent microwave circuit. The high-power paths are shown in red for properly phased sources ($\Delta\phi = \pi/2$).

sion loss for the perpendicular polarization is too small to measure.

Figure 17(b) shows a polarization filter. The wire grid is supported on a rectangular frame that slides into a grooved channel for easy insertion and removal. The wires for the PP filter are perpendicular to the long axis of the rectangular frame, and the wires for the OP filter are rotated 45° from this axis.

The Two-Tube Combiner

The final phase in the sensitivity enhancement program is to combine two of the new Varian 50-kW traveling-wave tubes. This is accomplished with the quasi-optical two-tube combiner illustrated in Figure 18(a). Figure 18(b) shows the microwave analogy, which uses a 3-dB sidewall coupler. For both cases, two properly phased inputs (with a phase differential of $\pi/2$) are combined as indicated. A quarter-wavelength-thick dielectric disk oriented at 45° to the beam becomes a broadband 3-dB hybrid if the dielectric constant ε equals 3.4 [19]. A quartz disk, which is perforated with a pattern of small holes to bring the dielectric constant down to the required value, serves as the quasi-optical hybrid. The beam waists from the two beam launchers intersect approximately at the quartz disk, although the only requirement for efficient combining is that the two input beams be symmetrical about the hybrid. Combining loss caused by tube unbalance is very forgiving (e.g., loss is less than 0.1 dB with phase differentials of ±20° or amplitude unbalance of ±2.5 dB). In common with most quasi-optical devices, the power-handling capability, bandwidth, and loss of the two-tube combiner are significantly improved over the waveguide equivalent.

The quasi-optical water-cooled load is an ALN disk matched to a water-filled cavity that is oriented at 45° to the incident beam, as indicated in Figure 18(a). This load reduces the level received by the horn by 10 dB; it can be reduced further by adjusting the wire-grid aperture cap. This configuration provides an adjustable range for the signal in the null monitor, which is used with the remotely controlled phase shifter in the drive circuit of one of the tubes to adjust and monitor phase balance. The system can operate efficiently with a single tube by either removing the quartz disk or replacing it with a metal plate, depending on which tube is activated.

The laser-alignment system uses small diameter (approximately 0.25 in) optical-quality mirrors imbedded in the reflectors. The mirrors are flush with the reflector surface, centered at the origin, and parallel to the x-y plane of the coordinate system used to define the reflector surface. Hence the laser beam is coincident with the beam axis (the central ray) throughout the BWG system. Figure 19 shows the completed two-tube combiner package with two HeNe lasers attached to the power-input ports. The quartz disk is replaced by an optical beam splitter for the alignment. The combined laser beams are directed

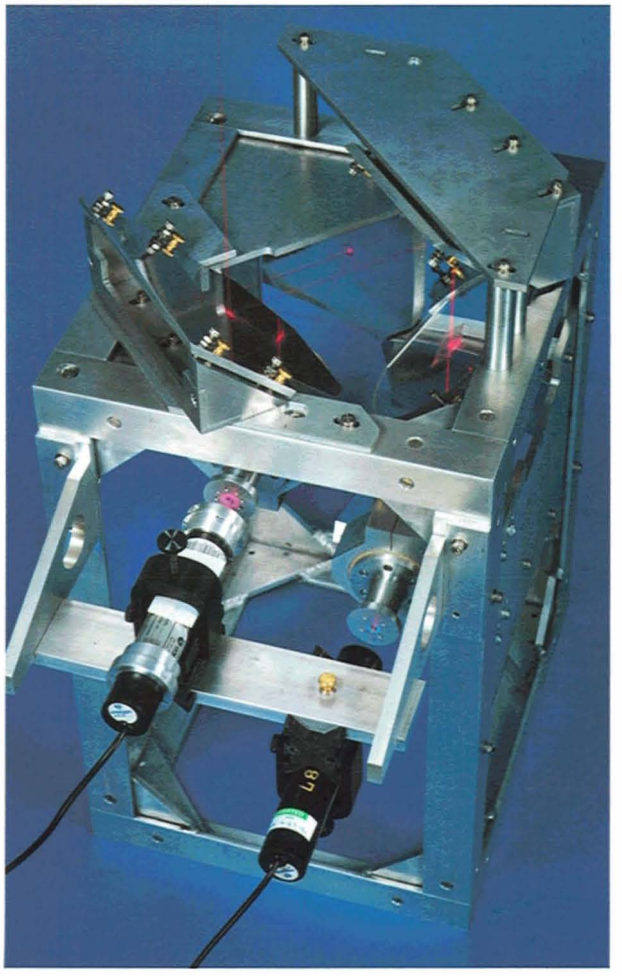

FIGURE 19. The two-tube combiner during laser alignment. The two superimposed laser beams directed upward represent the combined output, while the two superimposed beams to the right represent the dummy load.

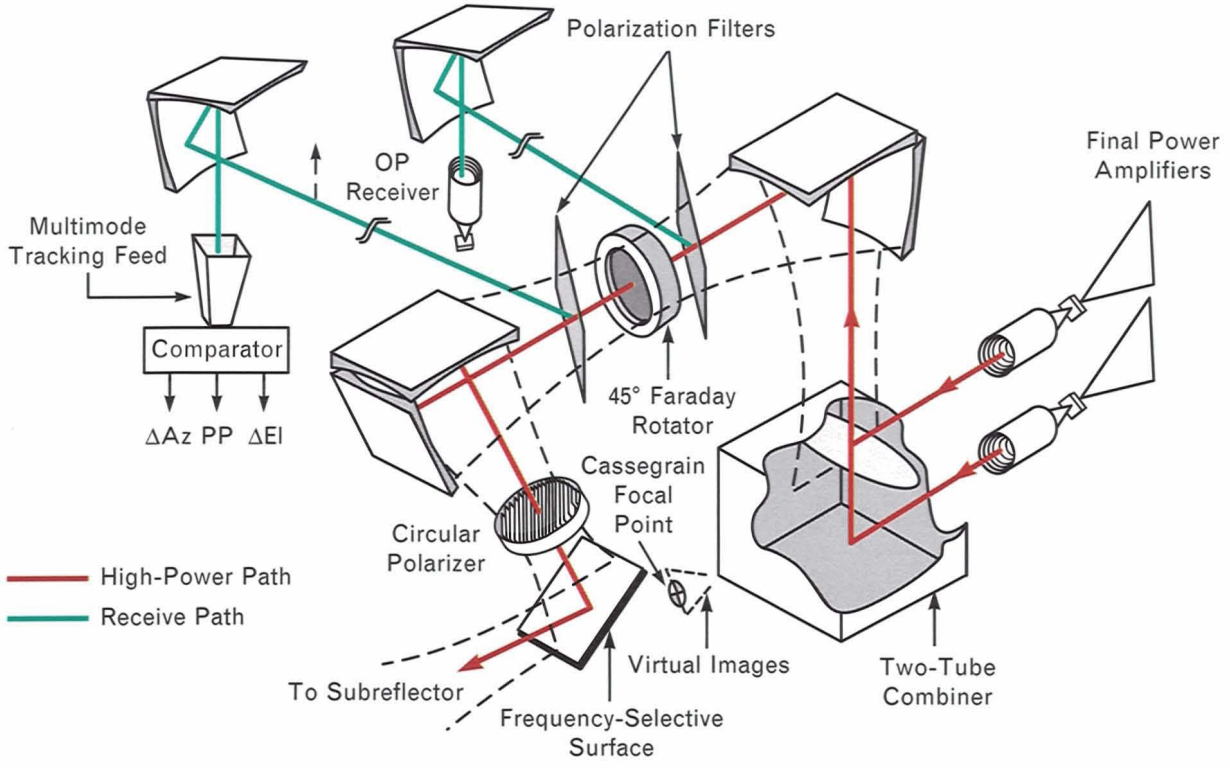

FIGURE 20. The system configuration of the various quasi-optical components. The high-power PP and OP beams have virtual images at the Cassegrain focal point. The system is functionally equivalent to the simplified diagram shown in Figure 3.

upward (representing the combined beam) and to the right (representing the dummy-load input of Figure 18(a)). Two plane reflectors in the combined beam path divert the output beam to place it in the desired high-power beam path.

Assembly, Alignment, and Test

Figure 20 illustrates the overall configuration of the BWG system. The system functions exactly as indicated in the simplified diagram in Figure 3. The clamshell reflectors periodically refocus the beam to define the BWG transmission paths. Three beam waists are in the high-power path; the first is at the two-tube combiner, the second is at the Faraday rotator, and the third is at the circular polarizer. The frequency-selective surface is a dichroic plate that reflects 35-GHz signals and passes 95-GHz signals. The beam waist at the circular polarizer is imaged by the frequency-selective surface at the Cassegrain focal point. Looking back from the subreflector, the system, in effect, sees three virtual images at the focal point. These images are the two-tube combiner output (the high-power channel), the multimode feed aperture (the PP receive channel), and the beam launcher representing the OP channel. Lateral displacement of any of these virtual images results in secondary beam scan. Hence poor alignment of the three individual beam paths can cause the secondary beams to be misaligned in space. This problem cannot occur in a conventional microwave system in which all transmit and receive beams spring from a common source (i.e., the multimode feed). Precision alignment is accomplished by using the laser-alignment technique and then verified with phase-center measurements on the antenna test range.

Three beam launchers are in the system; two are in the two-tube combiner and one is for the OP receiver. The beam launcher for the OP receiver uses different design parameters to place the input beam waist at the Faraday rotator. The reflector pair used with the

multimode feed is symmetrical, the input beam waist is partway between the polarization filter and the reflectors, and the output beam waist is at the multimode horn aperture. The angle-tracking modes, principally the TEM_{01} mode, traverse the path from the frequency-selective surface to the multimode horn aperture, where they are converted to the TE_{20} and LSE_{11} waveguide modes. Preserving mode purity along this path is critically important for good angle-tracking characteristics.

Figure 21 shows the support frame of the BWG system during assembly, with a single beam launcher, the clamshell reflectors, and the frequency-selective surface plate in position (the high-power path). The cylindrical HeNe laser is supported on a fixture pinned to the frame for easy removal and replacement without introducing errors in the pointing angle. The receive channels are aligned by replacing the polarization filters with a rectangular plate that has a mirror on the beam axis. During installation of the completed BWG assembly on the MMW antenna vertex plate, the cylindrical laser is reversed 180° and the frame is shimmed to position the laser beam at the center of the subreflector. This alignment accurately positions the virtual feeds in the MMW antenna system. Over a long period of time, the laser fixture can be easily reinstalled to check the alignment of the virtual feeds if modifications are made or if any mechanical mishaps occur.

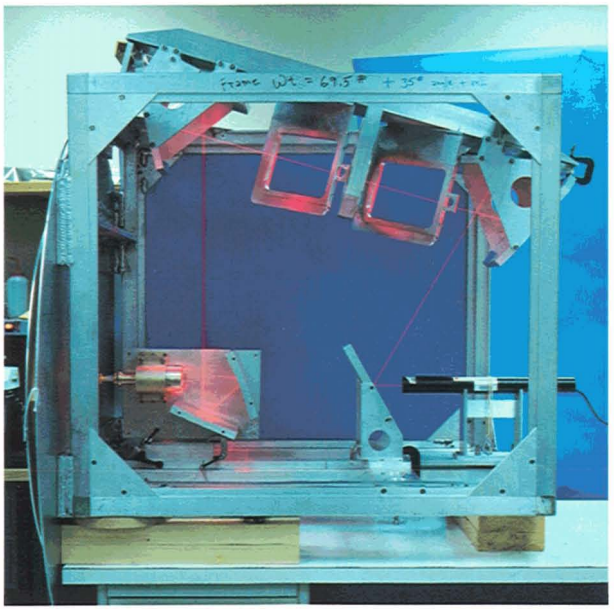

FIGURE 21. Laser alignment during assembly of the BWG system. The laser is directed at the frequency-selective surface to align the high-power path as well as the receive paths. When the BWG system is installed on the MMW antenna system, the alignment is accomplished by reversing the laser 180° to point at the center of the subreflector.

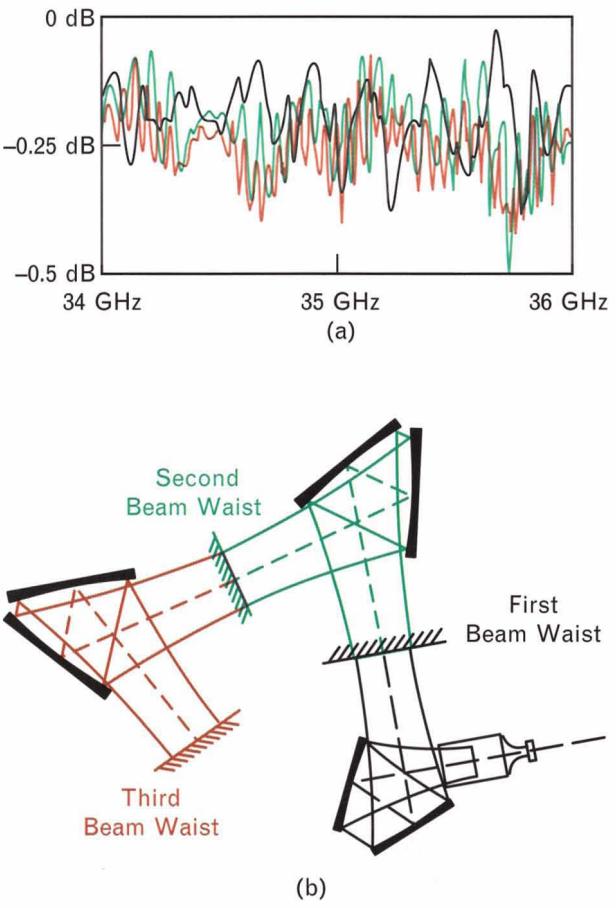

FIGURE 22. (a) Measured high-power channel losses from scalar horn input. (b) The shorting plate is successively placed at each of the three beam waists for the return loss measurements.

Figure 22 shows the radio-frequency transmission losses measured in the high-power channel. A plane reflector, or *shorting plate*, is placed at the output beam waist of the beam launcher for a return-loss measurement. The reference for the measurement is a short at the waveguide input to the scalar feed. The ripples of approximately ±0.1 dB come from the second-order Gaussian-Laguerre mode generated by the scalar feed and its input match (the voltage stand-

ing-wave ratio is approximately 1.15 to 1). Errors in this measurement lead to measured losses greater than actual because of the two-way phase errors in the higher-order mode. The shorting plate is next placed at the beam waist of the Faraday rotator, as shown in Figure 22(b), to determine the green curve in Figure 22(a), and then at the beam waist of the circular polarizer to determine the red curve. The additional loss between the beam-launcher output and the circular-polarizer beam waist (a distance of approximately 5 ft) is barely discernible.

Figure 23 shows representative primary pattern measurements. The distributions are approximately Gaussian with edge illumination of –12 dB; no cross-polarized energy above –40 dB was observed. Both *E*-plane and *H*-plane patterns were taken with the circular polarizers and the Faraday rotator removed. Phase measurements taken after final alignment show that the lateral displacement between the phase centers of the three virtual-image feeds is less than $\lambda/3$. This distance represents less than 1/20 of a beamwidth of secondary scan. The axial positions are within 2λ to 3λ of the Cassegrain focal point, which has a negligible effect on gain because of the large depth of focus of a high-magnification Cassegrain system. Relative gain measurements were made by using a large scalar feed with a beamwidth comparable to the BWG patterns as a gain standard. Results showed that the loss for both receive channels and the high-power channel was 0.3 ± 0.1 dB.

With the microwave system, the isolation between the high-power channel and the receive channel is typically –20 dB, because of component mismatches and low circulator isolation. The receivers must be protected against this high level of leakage during transmit time. Three-stage gas-tube receiver protectors that added 1.5 dB of loss at the receiver front ends were required. A significant advantage of the BWG system is its isolation characteristics. The measured isolation is in the range of –55 to –60 dB for the PP channels. The OP channel isolation is less because of reflections from the Faraday rotator, but it still has a measured isolation in the range of –35 to –40 dB. Reflections from the subreflector on transmit are theoretically only –42 dB. This return is dispersed by placing a cone at the center of the subreflector, with a base diameter small enough to be within the existing shadow blockage. The high isolation enables the gas-tube devices to be replaced with switchable ferrite circulators, which are capable of handling lower power levels with a loss of only 0.15 dB.

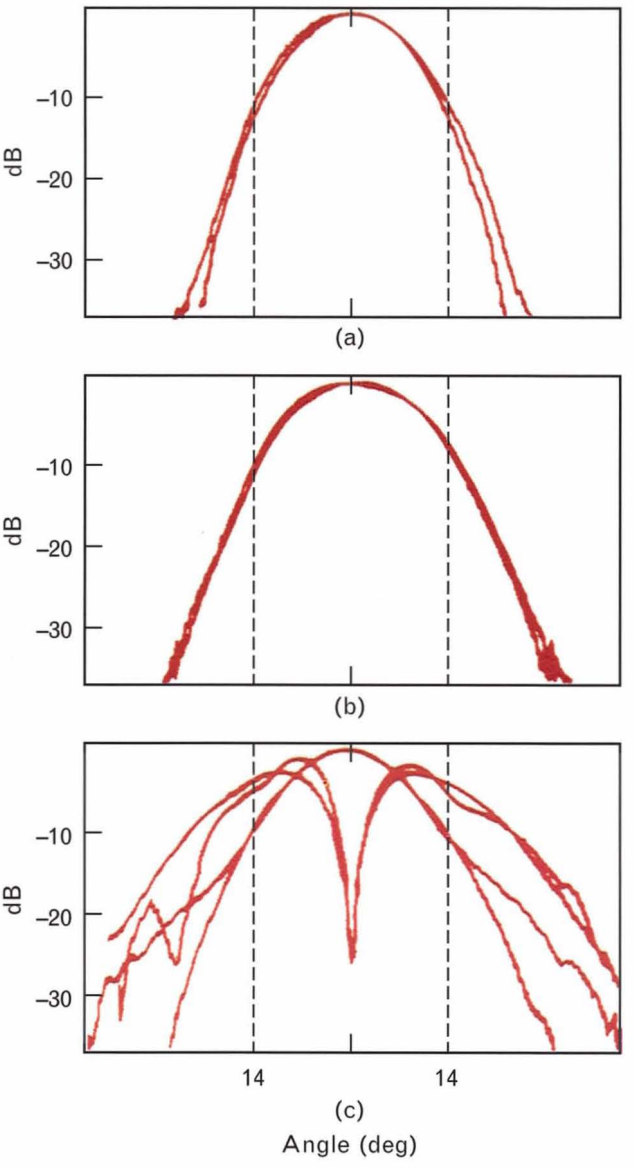

FIGURE 23. Primary patterns for (a) the high-power channel, (b) the OP channel, and (c) the PP channel. Cross-polarization is everywhere less than –40 dB. The vertical lines indicate the 14° angle subtended by the subreflector.

The 95-GHz feed must have its phase center coincident with the Cassegrain focal point, as shown in Figure 4. Sufficient space was reserved around the focal point to permit a future implementation of a

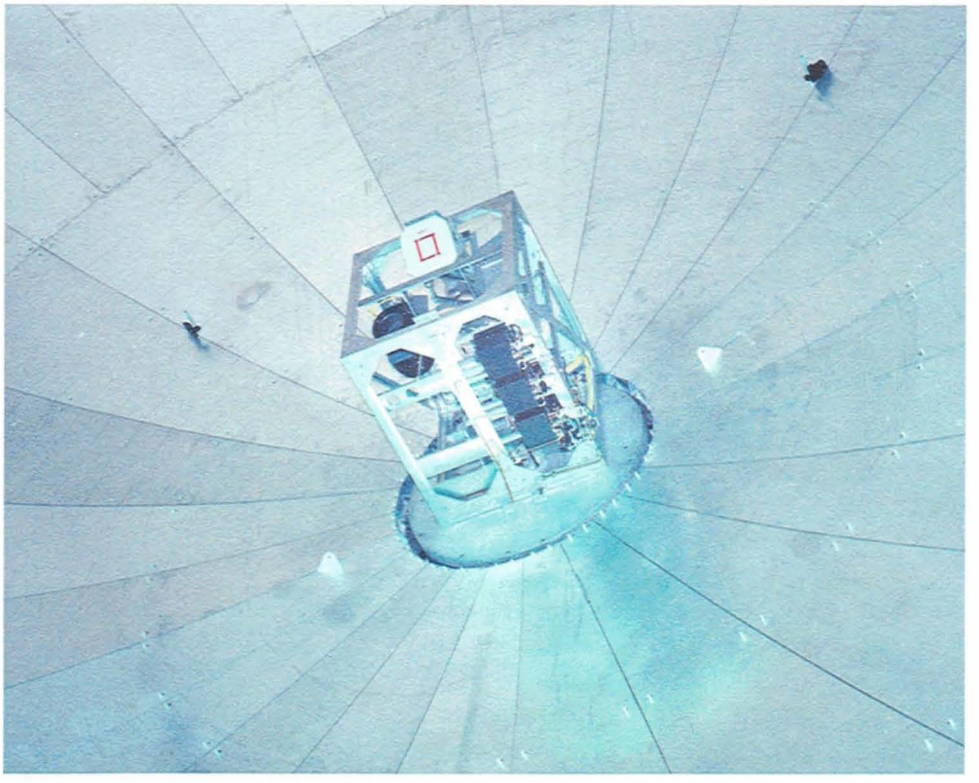

FIGURE 24. The BWG installed on the MMW antenna. The black boxes are the receiver front ends.

95-GHz BWG system.

System Evaluation

Figure 24 shows the completed BWG system installed on the MMW antenna. The frame was shimmed to direct the laser beam at the subreflector center and then bolted in place. The rectangular black boxes on the underside of the frame are the receiver front ends. The interface with the input waveguides, receiver lines, and control cables is at the center of the vertex plate. Figure 25 is a photo taken inside the radome showing the BWG system in position at the vertex of the main reflector, and the subreflector with the dispersing cone for reducing transmit leakage to the receive channels at its center.

System evaluation used well-established site proce-

Table 2. Sensitivity Improvement from Loss Reduction

Waveform	Gas-Tube Receiver Protectors	Switchable Ferrite Receiver Protectors
6 MHz	+2.35 dB	+4.1 dB
12 MHz	+2.07 dB	+3.82 dB
500 MHz	+1.97 dB	+3.72 dB
1000 MHz	+3.40 dB	+5.15 dB

dures to determine sensitivity, range and angle biases, and isolation. Balloon-borne calibration spheres were the principal means used to evaluate the sensitivity and pattern characteristics of the radar. A tower-mounted reflector on Gagan Island located 13 km from the radar was also utilized [20, 21].

Table 2 lists the improvement in sensitivity of the BWG system over the microwave system for the various waveforms without any increase in power output. These data are averaged over fifteen sphere tracks. The first column is the measured sensitivity improvement with the gas-tube receiver protectors installed. In the future, replacing these devices with switchable ferrite circulators will result in an additional 1.75-dB improvement by eliminating the gas-tube and waveguide losses. The high isolation of the BWG system between the transmit and receive channels makes the lossy gas-tube receiver protectors unnecessary. The

FIGURE 25. An inside view of the radome of the MMW antenna system, showing the BWG system at the vertex of the main reflector, and the subreflector with the dispersing cone at its center.

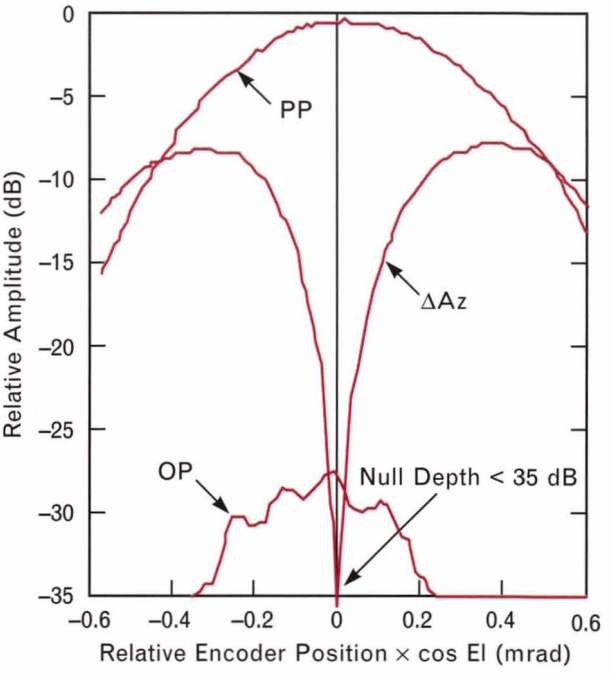

FIGURE 26. Typical two-way antenna patterns taken with balloon-borne calibration spheres.

sensitivity improvement is a nominal 4.0 dB for the narrowband waveforms and 5.0 dB for the 1.0-GHz waveform. The additional 1.0-dB improvement for the 1.0-GHz waveform corrects a long-known but unexplained deficit with this waveform; all waveforms now have approximately the same single-pulse sensitivity. The improvements listed in Table 2 are solely the result of reducing the microwave transmit and receive channel losses.

At this writing, the two new Varian tubes in parallel have produced power levels of 60 kW peak and 5 kW average. As soon as a power-supply limitation is corrected, power levels greater than 100 kW peak and 10 kW average are expected.

Figure 26 presents typical two-way patterns taken with a balloon-borne calibration sphere. These data are taken by using long-established site-calibration procedures in which a second radar assists by keeping track of the precise sphere location while the radar under test (the MMW in this instance) scans across the sphere and records two-way pattern characteristics. Null depths and overall balance in the difference channels is excellent; the PP-to-OP ratio (the polarization isolation between the two receive channels) is improved by 3 to 5 dB.

Summary

The MMW BWG is the first quasi-optical radar for the microwave region. Significant advantages of this system include reduced losses, increased bandwidth, and higher power-handling capability. Some of these advantages are

1. The increase in sensitivity achieved by reducing transmit and receive line losses is 4 to 5 dB.
2. Power levels of 60 kW peak and 5 kW average have been demonstrated without incident. Temperature sensors on the Faraday rotator magnet show no appreciable temperature rise.
3. Bandwidth has been increased from 1.0 to 2.0 GHz. The final power amplifier imposes the 2.0-GHz limitation. A new signal processing system is in development to utilize the increased bandwidth.
4. Antenna patterns show excellent null depths and difference-pattern symmetry.
5. The polarization isolation (i.e., the ratio of OP to PP returns from a calibration sphere) is typically –27 dB, which is an improvement of 3 to 5 dB over the microwave system.
6. The bandpass characteristics of the 1.0-GHz waveform are significantly improved.

The objective of the BWG program was to increase the single-pulse signal-to-noise ratio by 10 dB (4 dB via loss reduction and 6 dB by an increase in power). This goal will be achieved and perhaps exceeded when the new Varian tubes are fully utilized. Power-supply problems have delayed full-power generation. If subtle problems or disadvantages exist with the BWG system, they have yet to surface.

The quasi-optical components have exceptional performance characteristics when compared to their microwave analogs. Some of these performance characteristics are

1. The quasi-optical circulator, which has excellent transmission and isolation characteristics, makes possible radars with power levels that waveguide circulators cannot accommodate. The average power level of 5 kW already achieved by these quasi-optical circulators represents an order of magnitude increase over the level that burnt out the waveguide circulators.
2. The clamshell reflectors refocus the beam each iteration with the mode purity required for precision angle tracking (i.e., they produce extremely low levels of undesired mode coupling).
3. The beam launcher is an efficient transducer between the waveguide and a Gaussian beam. It gives the designer flexibility in the choice of horn size, beamwidth, and beam-waist location.
4. The BWG configuration permits the use of a much simplified low-power linearly polarized tracking feed. This simplification results in advantages in efficiency, bandwidth, and cost. In addition, the tracking feed eliminates the cross-polarized cross-coupling in the error channels, which causes problems with depolarizing off-axis targets.

The 95-GHz MMW radar and the Haystack Auxiliary radar (HAX), which is a high-power Ku-band system with a 13% bandwidth, will both employ BWG designs. Higher-power and broader-band components such as Faraday rotators and circular polarizers are under development in support of these programs.

A rule of thumb for a Cassegrain system, based on space available about the main reflector vertex, is that if the diameter of the main aperture is greater than 400 wavelengths, then a BWG system becomes a viable option. Electrically smaller apertures would result in increased shadow blockage by the BWG package. If the main aperture is an offset section of a paraboloid, there is (in principal) no low-frequency limit. A VHF quasi-optical circulator, however, would be something of a breakthrough.

Acknowledgments

I would like to express my appreciation to the Field Systems Group and the Radar Measurements Division at Lincoln Laboratory for their unwavering support and encouragement; Ed Chateauneuf and Dick Hogan for their mechanical design expertise; Felix Cramer and Ed May—both of whom are with General Electric at KREMS—who traveled far to provide invaluable mechanical and system integration assistance; John Magnuson and John Orthmann for their efforts at assembly, test, and installation; and Bill Piacentini and Dave Wilson for laboratory assistance.

REFERENCES

1. K.R. Roth, M.E. Austin, D.J. Frediani, G.H. Knittel, and A.V. Mrstik, "The Kiernan Reentry Measurements System on Kwajalein Atoll," *Linc. Lab. J.* **2**, 247 (1989).
2. C. Goubau and F. Schwering, "On the Guided Propagation of Electromagnetic Wave Beams," *IRE Trans. Antennas Propag.* **9**, 248 (May 1961).
3. J.E. Degenford, M.D. Sirkis, and W.H. Steier, "The Reflecting Beam Waveguide," *IEEE Trans. Microwave Theory Tech.* **12**, 445 (1964).
4. D.J. Sommers, L.I. Parad, and J.G. DiTullio, "Beam Waveguide Feed with Frequency-Reuse Diplexer for Satellite Communication Earth Station," *Microwave J.* **18**, 51 (Nov. 1975).
5. B. Claydon, "Beam Waveguide Feed for a Satellite Earth Station Antenna," *Marconi Rev.* **39**, 81 (1976).
6. D. Marcuse, *Light Transmission Optics* (Van Nostrand Reinhold, New York, 1972).
7. P.F. Goldsmith, "Quasi-Optical Techniques at Millimeter and Submillimeter Wavelengths," *Infrared and Millimeter Waves, Vol. 6,* ed. K. Button (Academic Press, New York, 1982), p. 277.
8. J.C.G. Lesurf, *Millimeter Wave Optics Devices and Systems* (A. Hilger, Bristol and New York, 1990), p. 13.
9. M.J. Gans, "Cross-Polarization in Reflector Type Beam Waveguides and Antennas," *Bell Systems Technical J.* **55**, No. 3, 289 (Mar. 1976).
10. B.M. Thomas, "Design of Corrugated Conical Horns," *IEEE Trans. Antennas Propag.* **26**, 367 (Mar. 1978).
11. R.J. Wylde, "Millimetre-Wave Gaussian Beam-Mode Optics and Corrugated Feed Horns," *IEE Proc.* **131-H**, 258 (1984).
12. D.C. Weikle, "Earth Coverage Corrugated Horns (44.5 GHz and 20.7 GHz)," *Technical Report 656,* Lincoln Laboratory (July 1983), DTIC #AD-A133241.
13. G.P. Rodrigue, "Circulators From 1 to 100 GHz," *Microwave J., State of the Art Reference* **32**, 115 (Supplement, Sept. 1989).
14. G.F. Dionne, J.A. Weiss, G.A. Allen, and W.D. Fitzgerald, "Quasi-Optical Ferrite Rotator for Millimeter Waves," *IEEE MTS-S Int. Microwave Symp.* **1**, *New York, 25–27 May 1988,* p. 127.
15. B. Lax and K. Button, *Microwave Ferrites and Ferrimagnetics,* (McGraw-Hill, New York, 1962).
16. K.R. Goudey and A.F. Sciambi, "High Power *X*-Band Monopulse Tracking Feed for the Lincoln Laboratory Long-Range Imaging Radar," *IEEE Trans. Microwave Theory Tech.* **26**, 326 (1978).
17. S.B. Cohn, "Flare Angle Changes in a Horn as a Means of Pattern Control," *Microwave J.* **13**, 41 (Oct. 1970).
18. P.F. Goldsmith, *op. cit.*, p. 320.
19. F.A. Benson, *Millimetre and Submillimetre Waves* (Iliffe Books, London, 1969).
20. E.G. May, "Site Evaluation of Beam Waveguide Feed," *Technical Memo No. AM0243,* General Electric Systems Division (14 Feb. 1990).
21. E.G. May, "Dipole Calibration with Beam Waveguide Feed," *Technical Memo No. AM0229,* General Electric Systems Division (16 Jan. 1990).

WILLIAM D. FITZGERALD
is a staff member in the Field Systems group. He received an S.B. degree in electrical engineering from MIT in 1956. From 1956 to 1961 he was an engineer with Chu Associates in Littleton, Mass. He has been at Lincoln Laboratory since 1961, and his principal activities have been with radio-frequency systems, reflector and array antennas, and microwave components. He has participated in the development of a number of radar systems, including the LR1R X-band radar at the Haystack facility, and the ALCOR C-band radar and the dual-frequency millimeter-wave radar at the Kwajalein Test Range in the Marshall Islands, where Bill has had two tours as a systems engineer. His most recent activities have been with hybrid (i.e., reflector/array limited scanning) systems and beam waveguide systems. Bill retired from Lincoln Laboratory in 1991 and is now enjoying an entrepreneurial adventure as the president of Microwave Beam Systems, Inc.